Negative redox potential shift in fire-retardant electrolytes and consequences for high-energy hybrid batteries

Bruno Ernould, Louis Sieuw, Gabriella Barozzino-Consiglio, Jean-François Gohy and Alexandru Vlad*

Institute of Condensed Mater and Nanosciences, Universite catholique de Louvain, Louvain-la-Neuve, Belgium.

Fire-retardant electrolyte chemistries have attracted great attention given their potential to solve the grand challenges of alkali-ion batteries : safety, use of metallic anodes and anodic stability. Whereas extensive analysis and correlations are drawn to explain their unusual electrochemical behaviour, one essential property, their effects on redox potentials of battery components (redox potential shift) pervasively lack a strict description and quantification. Here we show that the strong solvation of lithium cations by organic phosphates, the widely used flame-retardant constituents, induces a negative redox potential shift by as much as 500mV. We demonstrate that the redox potential shift is characteristic of Li-cation (de)solvation processes whereas negligible for other processes. This has important consequences for high energy hybrid battery concepts such as high voltage dual-ion graphite or organic batteries. These findings also shine a different light on the enhanced anodic stability of these non-conventional battery electrolyte formulations.

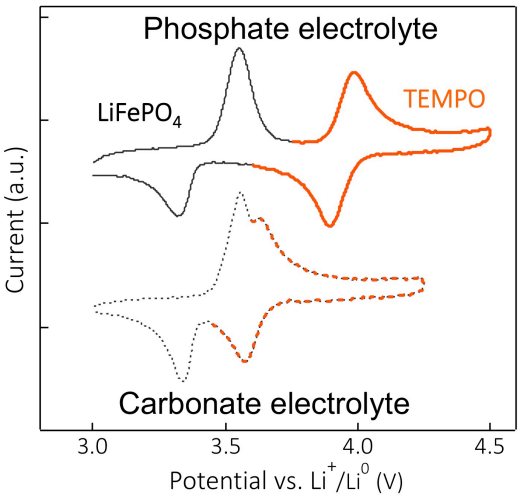

Introduction

Lithium-ion battery technology has definitely settled the concept as the solution of choice for small to large-scale energy storage systems.[1] Whereas Li-ion batteries are already a great commercial success, with exponential increase predictions owing in particular to automotive industry demand, further specifications improvements are highly sought. Continuous optimization of energy density, power, safety and costs relies on a complex interplay between finding higher energy active electrode materials, higher stability and safer electrolytes.[2-6]

From the early stages of battery developments, carbonate solvents have been used to dissolve $LiPF_6$ salt providing electrolytes with optimal ionic conductivities, viscosity and surface passivation properties.[7] Due to necessity of further development of the Lithium-ion batteries, other electrolyte properties such as high voltage stability, anode and lithium metal passivation, as well as safety regulations have been brought to the fore over the recent years. These have however required non-incremental changes of the electrolyte chemistry. Yet changing the electrolyte composition implies systematic differences in the Li-cation (Li^+) (de)solvation energies, bulk transports and interfacial transfer kinetics. In a battery, processes occurring at the interfaces will be affected if the solvation structure of Li-cation changes. The energy barrier for the transport of Li^+ at the liquid - solid interface might be closely related to the solvation ability of the solvents, and stripping off the last solvent molecule might be not only the rate-determining step but might also be affecting the electrochemical potential.

Recent developments draw particular attention to the redox potential when changing the electrolyte solvent,[8,9] with interestingly, the redox potential changes being measurable mainly for non (Li^+)-(de)solvation processes. The works of Nakanishi *et al*. and Leverick *et al.* detailing on the impact of solvent and salt concentration on the redox potential of the I^0/I^- redox mediator couple being noticeable recent examples.[10,11] Further considerations on this could also benefit from the reported redox potentials in various solvent environments measured with special electrochemical cell setups.[8,12-14] However, little is reported so far on the impact of these in Li-ion or Li-metal practical format cells.

While finalizing this work, Marinaro *et al.* published a complementary study on the influence of Li-salt concentration on the redox potential of lithium metal.[15] Whereas this report is based on measurements performed in a concentration cell design, and the only solvent analysed is the dimethyl sulfoxide, it provides a series of important findings that further corroborates with our results. First, it also shows that ferrocene can be used as a reliable and unambiguous internal reference. Furthermore, authors find a non-linear redox

potential dependence with salt concentration that cannot be estimated from simple consideration of Nernst equation. These points are also discussed in this work yet from a different perspective. Importantly, Marinaro's work further highlights the impact of the minor changes of the electrolyte chemistry on the redox potential.

With these considerations in mind, we focused our research on the impact of organic phosphate solvents on the redox potential values, what could be the consequences and how these can be further exploited. In particular, low molecular weight organic phosphates have been proposed as promising non-flammable solvents or electrolyte additives, because they possess similar physical and chemical properties to carbonates such as a wide range of operating temperatures, good solubility of Li salts, low viscosity and in particular, a wide electrochemical stability window.[2-5,16] High voltage stability was also observed, assigned either to improved cathode electrolyte interphase (CEI) or highest occupied molecular orbital / lowest unoccupied molecular orbital (HOMO/LUMO) bands offset for various applied phosphate chemistries.

However, the organic phosphates are also known for their strong coordination (solvation) ability toward alkali metal cations, in particular Li^+. This has been exploited for Li-cation extraction from brines.[17,18] Phosphate-lithium complexes can be also synthesized and isolated, further significative of strong binding of lithium cations.[19,20] Herein we show that this strong solvation (or coordination) ability of organic phosphate solvents induces a significant redox potential shift in the negative direction if the process is based on Li^+ (de)-solvation process. On the contrary, non-lithium redox processes are not affected. When set *vs*. a Li-based reference, higher voltages are then measured for non-lithium (de)-solvation processes. Such situations can notably be met in organic radical or dual-ion batteries, but also when dealing with the observation of enhanced anodic stability of electrolytes. We believe that this work will not only help designing safer high energy batteries but could also serve as a guideline for the evaluation of the redox potential at play in future battery and electrolyte chemistries.

Observing and quantifying the redox potential shift in presence of organic phosphates

Intrigued by experimental inconsistencies in our early work on organic radical batteries in lithium based organic phosphate electrolytes,[21] as well as literature survey,[22] we have initiated a project aiming at an in-depth analysis of the electrochemistry and determination of redox potentials in phosphate-based electrolytes, given their high affinity toward lithium cations.

To avoid any interference of the studied organic phosphate systems on the reference electrode (RE) potential, we have used non-Li pseudo-RE (Ag/AgCl). To further avoid any effect on the pseudo-RE of the phosphate, we have systematically used internal reference electrochemical system (RES) to calibrate the redox potential. A typical example obtained by using this pseudo-RE (Ag/AgCl) together with ferrocene (as RES) is shown in Figure 1.

The first noticeable fact is the negative shift of the Li^+/Li^0 redox potential (*vs.* Ag/AgCl) when replacing the propylene carbonate (PC) by trimethyl phosphate (TMP). Herein the intersection of the reduction and oxidation curves for the Li^+/Li^0 process was used to determine the redox potential of the Li^+/Li^0 couple.[23] This yielded results that have been also confirmed by Open Circuit Potential (OCP) measurements of non-polarized electrodes. A potential shift by as much as –260 mV *vs.* AgAgCl can be observed between the two electrolytes chemistries.

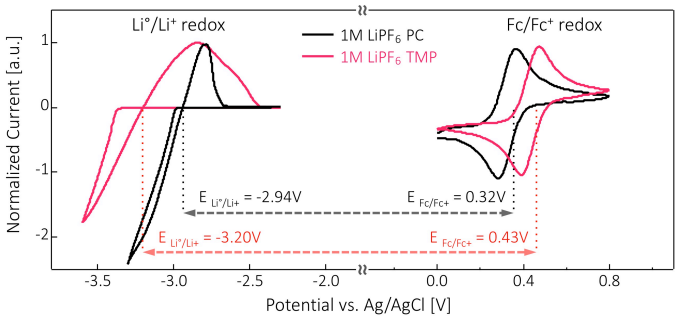

***Figure 1**. Cyclic voltammetry of the Li^+/Li^0 redox process measured in two different electrolyte solvents at 1 mV.s^{-1} (cathodic scan) with a Ni disc as WE, Li metal as CE and Ag/AgCl as pseudo-RE (propylene carbonate - PC and trimethyl phosphate - TMP). For the anodic scan (Fc/Fc^+ redox) the following conditions were applied: Ag/AgCl pseudo-RE, Pt disc as WE and Pt wire as CE; Fc concentration = 10 mM; scan rate = 25 mV.s^{-1}.*

Since redox potential was measured *vs.* Ag/AgCl pseudo-RE (refer to SI for experimental details), and that this reference is known to be sensitive to the electrolyte solvent composition,[24] we have calibrated the measured potential *vs*. ferrocene (Fc/Fc^+) RES, as also suggested by Marinaro's work.[15] The data shown in Fig. 1 indeed display different RE values for Ag/AgCl electrode as the Fc/Fc^+ redox is shifted by +110 mV. However, the shift is opposite to the Li^+/Li^0 redox and the combination of the two effects results in an overall shift of –370 mV for the Li^+/Li^0 redox when changing the solvent from PC to TMP.

Other pseudo-RE electrodes have been also used (Ag and Pt wire) with also other RES, such as $TEMPO/TEMPO^+$ redox. Whereas the relative values (*vs.* the pseudo-RE) were different as expected, the difference between the Li^+/Li^0 and internal reference redox was found consistently within the range of –400 mV ± 50 mV when changing the solvent from carbonates (EC, DMC, PC or mix of these) to TMP (refer also to Fig. 3 and S3). This confirms that the applied

methods are suitable for redox potential determination. To be further mentioned that Na^+/Na^0 redox potential has been found to shift when changing the solvents from carbonates to phosphates (Fig. S1). However, the lower magnitude of this shift being than for Li^+/Li^0 is explained by the lower solvation ability of Na^+ by phosphates.

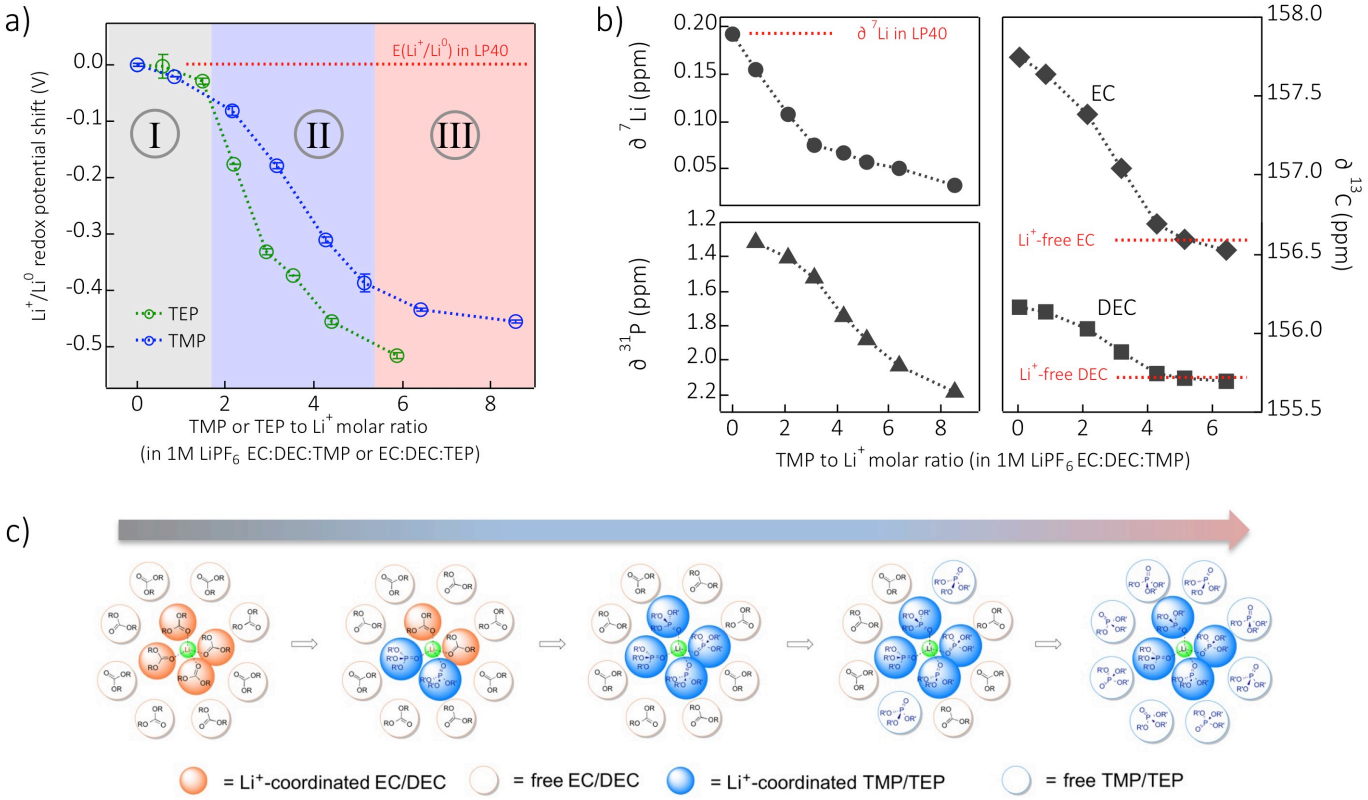

Figure 2. (a) Li^+/Li^0 redox potential shift as function of phosphate concentration while maintaining the concentration of $LiPF_6$ salt at 1 M in the EC:DEC:TMP or EC:DEC:TEP ternary solvent mixtures. The zero shift baseline corresponds to Li^+/Li^0 redox potential as measured in 1 M $LiPF_6$ in EC:DEC. (b) The corresponding ^7Li, ^{31}P and ^{13}C (carbonyl) NMR shift for the TMP-based electrolyte formulations. (c) Schematics of the rapid displacement of carbonates by phosphates in the Li^+-solvation shell as confirmed by redox potential shift (a) and NMR experiments (b).

Phosphate concentration impact and solvation shell structure

Intrigued by such a significative redox potential shift, we have undergone an extensive analysis of the impact of other phosphates (TMP and TEP) and their concentrations by measuring the redox potential shift (Fig. 2a) as well as the NMR chemical shifts of selected elements - ^7Li, ^{31}P and ^{13}C (Fig. 2b). The 1 M $LiPF_6$ in EC-DEC was used as baseline for all measurements.

The electrochemical shift analysis shows several interesting processes. First, the nature of the phosphate differently impacts the redox shift with higher values attained for TEP than TMP for the same phosphate-to-lithium molar ratio (Fig. 2a). This can be explained by the bulkiness of the alkyl moieties. As the steric hindrance of these moieties increases, the Li^+ centre is more efficiently shielded, yielding to higher stability of the solvated cation, which in turn further lowers the redox potential. This corroborates with the redox potential shift measured for other phosphorus-based chemistries (Fig. S2).

Trimethyl thiophosphate did not yield any significant shift (the shift being in fact positive, of about 30mV, Fig. S2) in comparison to phosphates, whereas trimethyl phosphine oxide induced an important shift. This also corroborates the knowledge that the Li-cation solvation proceeds primarily via the lone pair of oxygen atoms (in this case, of the phosphate group); but also that sulphur is poorly coordinating[19] the Li-cation. For instance, the trimethyl phosphine oxide does not contain other oxygen than the double bonded one to interact with the metal centre.

An interesting aspect is the "S"-shaped dependence of the redox potential shift with the increased phosphate ratio. Three distinct regimes can be identified, that can be explained through a modified Nernst equation potential change. This equation considers the Li^+ activity ($a_{Li,}$ equation 1) rather than Li-salt concentration (all being maintained at 1M in Fig. 2):

$$E = E° + \frac{RT}{nF}\ln(a_{Li}) \qquad \text{(eq.1)}$$

Lithium activity in turn is the result of a complex interplay between the dissociation of the cation solvation or ion-pair complexes present in solution (Fig. 2c) that can be broadly resumed to the following equations:

$$Li(SOLV)_x^+ A^- \rightleftharpoons Li^+ + xSOLV + A^- \qquad \text{(eq.2a);}$$

$$Li^+ + e^- \rightleftharpoons Li^0 \qquad \text{(eq.2b);}$$

Marinaro's work[15] effectively predicts the redox potential variation for different salt concentrations, with a rationale based on the concentration (activity) of free solvent molecules (DMSO in their respective case). Whereas their experimental and calculated values are in good agreement, we propose a different rationale. The solvent (SOLV) concentration will indeed affect the equilibrium of eq.2a so that at high SOLV concentrations (*i.e.* diluted salt regime) the equilibrium will be displaced to the left (eq.2a) resulting in low a_{Li} (eq.2b and eq.1).

In the ternary solvent system (EC-DEC-TMP) presented in Figure 2, the concentration of Li^+ salt is kept at 1 M, with total solvent-to-lithium molar ratios (Table S1) being well above the coordination number of lithium, broadly accepted of being around x≈<4.4 (in eq. 2a)[4] so that the transition from excess to limited free-solvent as presented by Marinaro *et al.*[15] cannot explain the large redox potential shift observed here.

The solvate complex dissociation constant in turn will effectively regulate the activity (eq.2a) and thus the redox potential E (eq.2b and eq.1). In the dilute phosphate region I, the solvation complexes are of $Li(DEC/EC)_x(TMP/TEP)_y$ general structure, where x+y≈4.4 and x>>y (Fig. 2c, Table S1). The lithium solvation environment is largely controlled by the carbonate species so that the redox potential is marginally affected. At the other extreme, region III, saturation is observed, and the strong solvation of phosphates displaces the eq.2 equilibrium toward lower a_{Li} and thus large negative redox potential shift according to eq.1 (E-E°<<0 V). The intermediate region II is certainly the most sensitive to the concentration of phosphate species with a redox potential shift of 300 to 400 mV in a narrow phosphate concentration window.

Additional hints on the solvation strength are provided by NMR analysis of the ternary EC-DEC-TMP electrolytes (Fig. 2b). From the carbonate group ^{13}C NMR shift (refer also to Fig. S4, Table S1) it can be noticed that at concentrations corresponding to a molar ratio of phosphate to lithium above 4.4, the EC and DEC are in the free, non-solvating forms, despite still being present in excess (TMP to total EC+DEC molar ratio of 0.7, refer to Table S1).

Also, increasing the phosphate concentration results in a ^7Li NMR signal upfield shift due to replacement of carbonates by phosphates in the Li^+ solvation sphere (Fig. S5). ^{31}P NMR chemical shift also follows a similar trend with the free phosphate being downfielded compared to the Li-coordinated species (Fig. S6). Whereas electronegativity would suggest a reverse trend, our data indicate that the Li-coordination by phosphates leads to an upfield shift of the ^{31}P signal because of a major degree of *d*-orbital occupancy in the P-O bonds once Li cation is coordinated to O=P.[25]

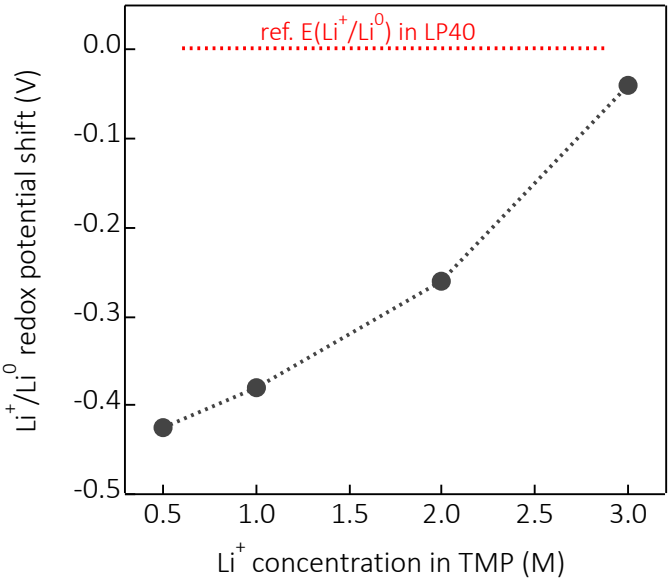

Figure 3. Redox potential shift as function of Li^+ salt concentration in TMP solvent.

In addition, DOSY NMR experiments have been also performed allowing us to determine the solvent coordination ratio of the different electrolytes as well as the lithium coordination numbers (see SI for details as well as Tables S6 and S7). The analysis shows that even at low TMP content, the amount of phosphate coordinated to Li^+ reaches values as high as 95% and for slightly higher concentrations of TMP, the carbonate molecules are mostly non-coordinated, further corroborating the ^7Li, ^{13}C and ^{31}P NMR data. Coordination number of Li^+ is found between 4 and 4.8 depending on the composition of the electrolyte, consistent with the reported values.[4] Thus, both NMR and electrochemical data interpretation support the strong solvation of Li^+ by organic phosphates, so that the weak dissociation of $Li(SOLV)_x^+$ complexes (eq.2a) leads to low a_{Li+} resulting in a negative redox potential shift (eq.1) when referenced to a weaker solvating electrolyte (LP40 here).

According to the analysis above, increasing the a_{Li}, should result in a positive increase of E (eq.1). This is expected to be achieved by also changing the concentration of the salt and the results of various Li-salt concentrations in TMP are shown in Fig. 3. Corroborating Marinaro's work, dealing also with strongly solvating DMSO electrolyte solvent, the redox potential shift does not scale at 59 mV/decade as expected from simple considerations of Nernst

equation. This is because the increase of salt concentration affects the lithium solvation complex structure (eq.2) and a_{Li} does not follow a linear trend with Li-salt concentration, in particular in strongly solvating solvents. At a salt concentration below 2 M, the phosphate to lithium molar ratio is above 4.3 (8.6 for 1 M, 4.3 for 2 M) and a_{Li} is low given the strong solvation by TMP. At higher salt concentrations, there is no sufficient solvent to saturate the solvation shell and ion pairing needs to be considered to properly estimate a_{Li}. Certainly, when considering strongly solvating systems, salt concentration effect should not be considered as a simple extension of dilute systems.

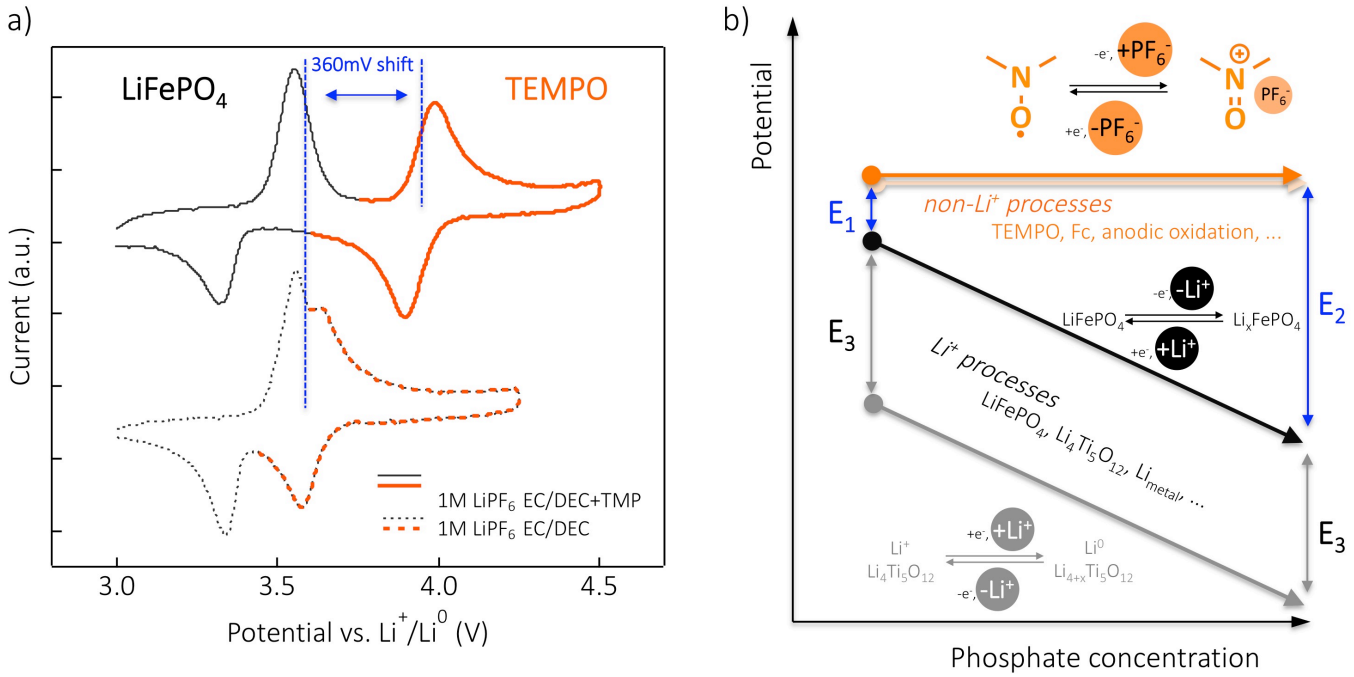

Figure 4. (a) Cyclic voltammetry of a hybrid PTMA/$LiFePO_4$ electrode measured in a two-electrode cell configuration, *vs.* lithium metal pseudo-reference with two different electrolytes: 1 M $LiPF_6$ in EC/DEC and 1 M $LiPF_6$ in EC/DEC/TMP. (b) Schematics of Li^+ *vs.* non-Li^+ (de)solvation redox differentiation. In the case of Li-ion cells, the influence of the solvent on the Li^+ chemical potential (or the redox potential E_3) can be considered as symmetrically affected at the positive and negative electrode interfaces.

Differentiating Li^+ vs. non-Li^+ (de)solvating processes

Whereas it is clear that phosphates can induce a large redox potential shift, it is worth recalling that all values reported above are based on non-Li RES (ferrocene, TEMPO). In other words, all RES used in this work rely on a redox mechanism that uses anions instead of cations for charge compensation. This led us to the hypothesis that all redox processes that operate through anion rather than Li-cation charge compensation will appear shifted if measured versus a Li-based pseudo-RE.

To examine this, we have constructed a series of hybrid active material electrodes and tested them with different electrolytes. We have intentionally designed active material electrodes that operate through different redox charge compensation: a Li-ion active material requiring Li^+-(de)solvation at the electrolyte-electrode interface (*e.g.* $LiFePO_4$ and $Li_4Ti_5O_{12}$); and a nitroxide radical (TEMPO) containing polymer (PTMA) that relies on anion and not Li-cation charge compensation during redox.

A typical set of results is shown in Fig. 4a. The cell configuration was a two-electrode, with PTMA/LFP[26] working electrode, and Li metal CE and pseudo-RE. With such configuration, the measured cell voltage (or as typically reported potentials *vs.* Li^+/Li^0) is the difference between the electrode potentials of the WE and of the pseudo-RE.

The PTMA and LFP constituent responses in the two sets of electrolytes are strikingly different. There is no apparent effect on the redox potential for the $LiFePO_4/FePO_4$ couple, with a half wave redox potential at 3.42 V, that is widely acknowledged as the equilibrium redox potential of $LiFePO_4$ (when measured in a lithium cell). Markedly however, the half wave redox potential of PTMA increases by as much as 360 mV when in presence of 50 vol% TMP: from 3.61 V (vs. Li^+/Li^0 in 1 M $LiPF_6$ EC/DEC) up to 3.96 V (vs. Li^+/Li^0 in 1 M $LiPF_6$ EC/DEC+TMP). While the former is widely acknowledged as the redox potential of the nitroxide couple measured in aprotic electrolytes (and referenced *vs.* Li^+/Li^0), the latter is unusually high.

The nitroxide surrounding molecular environment has been shown to affect the reactivity (and thus, presumably, the redox potential) of the nitroxide group.[27] Yet there are no reported interactions mechanisms with the organic phosphates, or other solvents, as to enable such a strong redox shift. Accordingly, another mechanism is responsible for such a high shift.

Based on the observations above, the following rationale is advanced (Fig. 4b):

(i) all redox processes involving lithium (de)solvation are affected by the solvation strength with the redox potential shift affected proportionally (as schematically depicted in Fig. 4b, where E_3 will remain constant). In the case of organic phosphates, as shown by the experiments detailed above, the shift is negative, lowering thus the redox potential (Figs. 1 and 2). Increasing the salt concentration reverses the trend (Fig. 3).

(ii) all redox processes that do not involve lithium (de)solvation are not affected by the solvation strength and their redox (or chemical) potential is barely affected or not influenced at all by the lithium-cation solvation strength or the salt concentration.

The analysis of data in Figures 1 and 2 further supports this hypothesis and the results presented in Figure 4 take a different signification in the light of these. The redox potential of PTMA is not up-shifting, and remains close to its nominal value, of 3.63 V (as for instance reported *vs.* Li pseudo-RE in carbonates electrolytes with 1M salt). In turn, the redox potential of $LiFePO_4$, but essentially, also of Li^+/Li^0 redox (used here as pseudo-RE) processes, are shifted to lower values. This results in no apparent redox shift of $LiFePO_4$, since the working and the pseudo-RE operate through symmetrical lithium (de)solvation; yet this results in an apparent increase of the redox potential of PTMA.

The redox potential shift function of solvation strength can be generalized also to other processes that either rely, or not, on lithium (de)solvation steps, or via a combination of both (Figs. 1 and 4b). The magnitude of the shift will be dependent on the nature of the solvent (Fig. 2) but also on the relative concentrations of both lithium salt and solvent (Fig. 3).

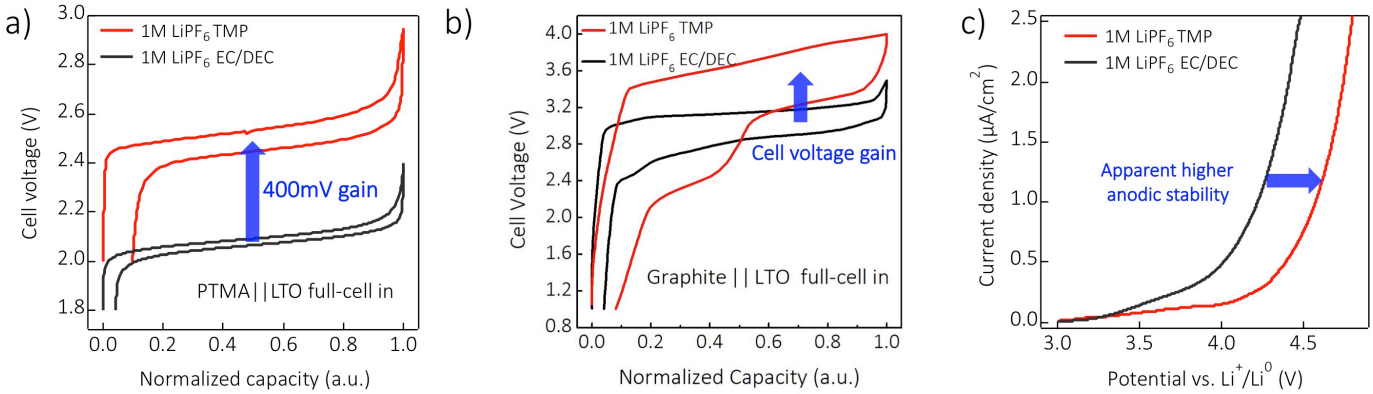

Figure 5. Voltage gain in dual-ion (a) PTMA-LTO and (b) graphite-LTO cells, as well as (c) increased apparent anodic stability by tuning the lithium cation solvation strength.

Impact and potential applications

Considering the potential general impact of these findings, we have further designed and studied electrochemical cells where the redox potential differentiation between lithium and non-lithium (de)solvation processes can lead to significative improvements.

The first set of experiments concerns the dual-ion battery chemistries (Fig. 5a, b) since these have asymmetric redox charge compensation mechanisms: Li^+ redox or (de)solvation at the anode and anion insertion at the cathode. The later implies no Li^+ (de)solvation at the cathode electrode interface so any redox potential shift induced by Li^+ solvation will not be measured here. In other words, the redox potential will not be affected for the nitroxide radical in the PTMA electrode (Fig. 5a), or for PF_6^- anion intercalation into graphite electrode (Fig. 5b). In turn, at the anode electrode side, since Li^+ (de)solvation is required, either for Li^+ intercalation in $Li_4Ti_5O_{12}$ (Fig. 5a,b), or for Li^+/Li^0 redox (Fig. S10) the solvation strength will shift the redox potential to lower values.

And as designed, we do increase the cell voltage of the cells when replacing the carbonate solvents by TMP. A PTMA-LTO cell has a nominal voltage of 2.07 V when operated in carbonate electrolytes. This is consistent with known and measured values for PTMA and LTO redox potential, when measured in 1 M salt carbonate electrolytes: 3.63 V and 1.6 V, respectively. When assembled with 1 M $LiPF_6$ in TMP electrolyte, an average cell voltage of 2.45 V is measured, that could be frenziedly assigned to some exotic interactions between the phosphate molecules and the nitroxide redox

centre. Yet according to our analysis, this is the result of shifting the chemical potential at LTO interface to lower values. A similar rationale applies for the graphite anion cell (Fig. 5b, S10) where the operational voltage window while changing the electrolyte chemistry and composition can lead to different performances as also observed in some recent reports.[28-31]

Another important consequence is the apparent enhanced anodic stability of the electrolytes, if the measurement is done *vs.* a Li-based pseudo-RE (Fig. 5c). In the absence of active Li-ion cathode materials, the reactions taking place at the working electrode under high anodic polarization is a complex interplay between the oxidation of anion salts, oxidation of solvent molecules as well as corrosion of current collector. These can be all treated as having the following general reaction equation:

$$A \rightarrow A^{+} + e^{-} \quad \text{(eq.3)}.$$

Important, in the light of our analysis above, we can expect lithium solvation strength to affect insignificantly the chemical potential of these oxidation processes since these are not based on Li (de)-solvation processes. Indeed, when performing a linear voltammetry scan on stainless steel electrode surface of the most significative electrolyte formulation examples in this work, we noticed enhanced anodic stability while increasing the amount of organic phosphate constituents. As shown in Fig. 5c, the onset[32] as well as the electro-oxidation amplitude are shifted to higher redox potential when comparing 1 M $LiPF_6$ in TMP to EC/DEC electrolyte systems. To note, the magnitude of the shift is comparable to the redox potential shift when in the presence of TMP (Fig. 2). Although surface passivation from TMP molecules could be also taken into account, the apparent increased anodic stability is rather the result of lowering the pseudo-reference lithium metal electrode potential in the strongly solvating environment.

Conclusions

In this work we show that the strong solvation of lithium cation by the flame-retardant organic phosphates has an important effect on the relevance of the measured electrochemical potentials if a non-adequate electrochemical configuration is employed. When both, working and pseudo-reference electrodes rely on lithium (de)solvation, the effect is not detectable since the redox potential shifts proportionally. The redox potential shift will thus remain elusive for any measurement set against the potential of a lithium-based reference process, independent whether a two or three-electrode set-up is used. The readings of the non-lithium processes however will be strongly affected, resulting in apparently higher redox potentials, with the amplitude of the shift being proportional to the solvation strength. The amplitude of the redox potential shift with the studied organic phosphates can be as high as –500 mV when compared to conventional carbonate-based electrolytes.

With further optimization on the cathodic stability as well as (de)solvation kinetics, these electrolyte systems could be further exploited to build high voltage dual-ion batteries. This could be also an interesting strategy to enable high voltage cathode chemistries and batteries. Although it may be a long way to realize such electrolytes in practical application after resolving the problems above, we believe that this peculiar electrochemical feature and the mechanism presented here will be of great value not only in the development of next-generation advanced batteries but also in the fundamental research in electrochemistry and solution chemistry.

Supporting Information

Additional electrochemistry data and experimental details.

Corresponding author

alexandru.vlad@uclouvain.be

Acknowledgments

Funding for this work was provided by grants FNRS - J.0043.18 - MESOPOL, FNRS - U.N011.18 - DEMIST, CF-ARC grants (18/23-093) MICROBAT and (14/19-057) BATTAB. A.V. is also indebted to the European Research Council (ERC) under the European Union's Horizon 2020 research and innovation program (grant agreement no. 770870) for partial financial support. We would also like to thank Q. Zhu and X. Zhang for their help with the dual-ion graphite battery tests.

References

(1) Dunn, B.; Kamath, H.; Tarascon, J.-M. Electrical Energy Storage for the Grid: A Battery of Choices. *Science* **2011**, *334*, 928–935.

(2) Liu, K.; Kong, B.; Chen, Z.; Liu, W.; Cui, Y.; Sun, Y.; Qiu, Y.; Lin, D.; Zhuo, D. Electrospun Core-Shell Microfiber Separator with Thermal-Triggered Flame-Retardant Properties for Lithium-Ion Batteries. *Sci. Adv.* **2017**, *3*, e1601978.

(3) Wang, J.; Yamada, Y.; Sodeyama, K.; Watanabe, E.; Takada, K.; Tateyama, Y.; Yamada, A. Fire-Extinguishing Organic Electrolytes for Safe Batteries. *Nat. Energy* **2018**, *3*, 22–29.

(4) Zeng, Z.; Murugesan, V.; Han, K. S.; Jiang, X.; Cao, Y.; Xiao, L.; Ai, X.; Yang, H.; Zhang, J.-G.; Sushko, M. L.; Liu, J. Non-Flammable Electrolytes with High Salt-to-Solvent Ratios for Li-Ion and Li-Metal Batteries. *Nat. Energy* **2018**, *3*, 674–681.

(5) Fan, X.; Chen, L.; Borodin, B.; Ji, X.; Chen, J.; Hou, S.; Deng, T.; Zheng, J.; Yang, C.; Liou, S.-C.; Amine, K.; Xu, K.; Wang, C. Non-Flammable Electrolyte Enables Li-Metal Batteries with Aggressive Cathode Chemistries. *Nat. Nanotechnol.*

2018, *13*, 715–722.

(6) Grey, C. P.; Tarascon, J. M. Sustainability and *in Situ* Monitoring in Battery Development. *Nat. Mater.* **2017**, *16*, 45–56.

(7) van Schalkwijk, W. A.; Scrosati, B. *Advances in Lithium-Ion Batteries*. Springer: Boston, 2002.

(8) Su, C.-C.; He, M.; Amine, R.; Rojas, T.; Cheng, L.; Ngob, A. T.; Amine, K. Solvating Power Series of Electrolyte Solvents for Lithium Batteries. *Energy Environ. Sci.* **2019**, *12*, 1249–1254.

(9) Kim, D.-H.; Hwang, S.; Cho, J.-J.; Yu, S. Kim, S.; Jeon, J.; Ahn, K. H. Lee, C.; Song, H. K.; Lee, H. Toward Fast Operation of Lithium Batteries: Ion Activity as the Factor To Determine the Concentration Polarization. *ACS Energy Lett.* **2019**, *4*, 1265–1270.

(10) Nakanishi, A.; Thomas, M. L.; Kwon, H.-M.; Kobayashi, Y.; Tatara, R.; Ueno, K.; Dokko, K.; Watanabe, M. Electrolyte Composition in Li/O_2 Batteries with LiI Redox Mediators: Solvation Effects on Redox Potentials and Implications for Redox Shuttling. *J. Phys. Chem. C* **2018**, *122*, 1522–1534.

(11) Leverick, G.; Tułodziecki, M.; Tatara, R.; Bardé, F.; Shao-Horn, Y. Solvent-Dependent Oxidizing Power of LiI Redox Couples for Li-O_2 Batteries. *Joule* **2019**, *3*, 1106–1126.

(12) Gritzner, G. Solvent Effects on Half-Wave Potentials. *J. Phys. Chem.* **1986**, *90*, 5478–5485.

(13) Gritzner, G.; Auinger, M. Statistical Analysis of Gibbs Energies of Transfer of Cations and Soft Solvent Parameters. *Acta Chim. Slov.* **2009**, *56*, 86–94.

(14) Okoshi, M.; Yamada, Y.; Yamada, A.; Nakai, H. Theoretical Analysis on De-Solvation of Lithium, Sodium, and Magnesium Cations to Organic Electrolyte Solvents. *J. Electrochem. Soc.* **2013**, *160*, A2160–A2165.

(15) Kottam, P. K. R.; Kalkan, D.; Wohlfahrt-Mehrens, M.; Marinaro, M. Influence of Li-Salt Concentration on Redox Potential of Lithium Metal and Electrochemistry of Ferrocene in DMSO-Based Electrolytes. *J. Electrochem. Soc.* **2019**, *166*, A1574–A1579.

(16) Jiang, X.; Liu, X.; Zeng, Z.; Xiao, L.; Ai, X.; Yang, H.; Cao, Y. A Bifunctional Fluorophosphate Electrolyte for Safer Sodium-Ion Batteries. *iScience* **2018**, *10*, 114–122.

(17) Shi, C.; Duan, D.; Jia, Y.; Jing, Y. A Highly Efficient Solvent System Containing Ionic Liquid in Tributyl Phosphate for Lithium Ion Extraction. *J. Mol. Liq.* **2014**, *200*, 191–195

(18) Shi, C.; Jing, Y.; Jia, Y. Solvent Extraction of Lithium Ions by Tri-*n*-Butyl Phosphate Using a Room Temperature Ionic Liquid. *J. Mol. Liq.* **2016**, *215*, 640–646.

(19) Olsher, U.; Izatt, R. M.; Bradshaw, J. S.; Dalley, K. N. Coordination Chemistry of Lithium Ion: A Crystal and Molecular Structure Review. *Chem. Rev.* **1991**, *91*, 137–164.

(20) Varnek, A. A. ; Morosi, G.; Gamba, A. Molecular Modelling of Organophosphorus Podands and Their Complexes with Alkali Metal Cations. *J. Phys. Org. Chem.* **1992**, *5*, 109–118.

(21) Ernould, B.; Devos, M.; Bourgeois, J.-P.; Rolland, J.; Vlad, A.; Gohy, J.-F. Grafting of a Redox Polymer onto Carbon Nanotubes for High Capacity Battery Materials. *J. Mater. Chem. A* **2015**, *3*, 8832–8839.

(22) Nakahara, K.; Matsumoto, K.; Iwasa, S.; Miura, S.; Morioka, Y.; Suguro, M. Electric Storage Device. JP5146049 (B2), 2013.

(23) Tchitchekova, D. S.; Monti, D.; Johansson, P.; Bardé, F.; Randon-Vitanova, A.; Palacín, M. R.; Ponrouch, A. On the Reliability of Half-Cell Tests for Monovalent (Li^+, Na^+) and Divalent (Mg^{2+}, Ca^{2+}) Cation Based Batteries. *J. Electrochem. Soc.* **2017**, *164*, A1384–A1392.

(24) Gritzner, G.; Kůta, J. Recommendations on Reporting Electrode Potentials in Nonaqueous Solvents. *Pure Appl. Chem.* **1984**, *29*, 461–466.

(25) Koo, I. S.; Ali, D.; Yang, K.; Park, Y.; Wardlaw, D. M.; Buncel, E. Theoretical Study of ^{31}P NMR Chemical Shifts for Organophosphorus Esters, Their Anions and *O*,*O*-Dimethylthiophosphorate Anion with Metal Complexes. *Bull. Korean Chem. Soc.* **2008**, *29*, 2252-2258.

(26) Vlad, A.; Singh, N.; Rolland, J.; Melinte, S.; Ajayan, P. M.; Gohy, J.-F. Hybrid Supercapacitor-Battery Materials for Fast Electrochemical Charge Storage. *Sci. Rep.* **2015**, *4*, 4315.

(27) Dardenne, N.; Hautier, G.; Gohy, J.-F.; Charlier, J.-C.; Rignanese, G.-M. Ab Initio Calculations of Open Cell Voltage in Newly Designed PTMA-Based Li-Ion Organic Radical Batteries. *Comput. Mater. Sci.* **2018**, *143*, 27–31.

(28) Kravchyk, K. V.; Bhauriyal, P.; Piveteau, L.; Guntlin, C. P.; Pathak, B.; Kovalenko, M. V. High-Energy-Density Dual-Ion Battery for Stationary Storage of Electricity Using Concentrated Potassium Fluorosulfonylimide. *Nat. Commun.* **2018**, *9*, 4469.

(29) Heckmann, A.; Thienenkamp, J.; Beltrop, K.; Winter, M.; Brunklaus, G.; Placke, T. Towards High-Performance Dual-Graphite Batteries Using Highly Concentrated Organic Electrolytes. *Electrochim. Acta* **2018**, *260*, 514–525.

(30) Placke, T.; Heckmann, A.; Schmuch, R.; Meister, P.; Beltrop, K. Winter, M. Perspective on Performance, Cost, and Technical Challenges for Practical Dual-Ion Batteries. *Joule* **2018**, *2*, 2528–2550.

(31) Zhang, L.; Huang, Y.; Fan, H.; Wang, H. Flame-Retardant Electrolyte Solution for Dual-Ion Batteries. *ACS Appl. Energy Mater.* **2019**, *2*, 1363–1370.

(32) Moshkovich, M.; Cojocaru, M.; Gottlieb, H. E.; Aurbach, D. The Study of the Anodic Stability of Alkyl Carbonate Solutions by *in Situ* FTIR Spectroscopy, EQCM, NMR and MS. *J. Electroanal. Chem.* **2001**, *497*, 84–96.

Supporting Information for

Negative redox potential shift in fire-retardant electrolytes and consequences for high-energy hybrid batteries

Bruno Ernould, Louis Sieuw, Gabriella Barozzino-Consiglio, Jean-François Gohy and Alexandru Vlad*

Institute of Condensed Mater and Nanosciences, Université catholique de Louvain, Louvain-la-Neuve Belgium.

Corresponding author : alexandru.vlad@uclouvain.be

Table of contents

1. Materials and Methods

Materials

Lithium metal foils purchased from Gelon. Trimethyl phosphate (TMP, 99%, Acros), triethyl phosphate (TEP, ReagentPlus, ≥99.8%), triphenyl phosphate (TPhP, 99+%, Acros), tributyl phosphate (TBP, ≥99%, Sigma-Aldrich), trimethylphosphine oxide (TMPOx, Alfa Aesar) and trimethyl thiophosphate (TMThP, Alfa-Aesar) were dried in vacuum before use. 2,2,6,6-Tetramethylpiperidine 1-oxyl free radical (TEMPO, >98.0%, TCI), ferrocene (Fc, Sigma-Aldrich), $LiPF_6$ (battery grade ≥99.99% trace metals basis, Sigma-Aldrich), LiTFSI (battery grade, Sigma-Aldrich), $NaPF_6$ (battery grade, Sigma-Aldrich) and all phosphorous-based chemicals are degassed under vacuum prior use in an argon filled glovebox. All electrolyte solutions were purchased from Solvionic and were used as received: EC/DEC 1:1 (v:v) 1 M $LiPF_6$; PC 1 M $LiPF_6$; EC/DEC 1 M $LiPF_6$; EC/DEC 1 M $NaPF_6$. 1-Butanol (99%, extra pure, Acros), MWCNT NC7000 (Nanocyl, Ltd.), copper wire (0.64 mm diameter, Puratronic, 99.999% metal basis, oxygen free, ≈ 2.87 g/m, Alfa Aesar), NMP (ACS Reagent, Acros), were used as received. Ag, Ni and Pt pseudo-RE disc electrodes (diameter 2mm), and Pt wire counter-electrodes, styrene-butadiene rubber (SBR) and carboxymethyl cellulose (CMC) are purchased from MTI Corp.

Methods

Cyclic voltammetry of the Li^+/Li^0 redox process.

This experiment was carried in a glovebox under argon. A beaker cell was loaded with the electrolyte solution, TMP 1 M $LiPF_6$. The first electrochemical test involved the following set of electrodes: a Ni disc as WE, a lithium chip stuck on a copper support as CE, Ag/AgCl in presence of NBu_4Cl (0.004 M) as pseudo-RE electrode. Using this setup, a linear scan voltammetry was performed at 1 $mV.s^{-1}$ (cathodic polarization) between –2.30 V and –3.60 V.

Next the calibration (anodic polarization) was carried out using ferrocene (2 mg/mL) added to the same electrolyte medium as reference electrochemical system, in combination with and a Pt disc WE, a Pt wire CE and same Ag/AgCl RE. The voltage window was scanned between 0.00 V and 0.80 V at 50 $mV.s^{-1}$.

The same two experiments were then carried out with PC 1 M $LiPF_6$ commercial electrolyte, only the voltage window for the cathodic polarization was adjusted to be –2.3 V to –3.3 V.

Cyclic voltammetry to study the Li-salt concentration effect

The same setup presented beforehand to study the Li^+/Li^0 redox process was used to evidence the voltage upshift effect via the variation of the Li^+ salt concentration in TMP. The electrolytes used here are based on LiTFSI, varying the concentrations thereof (0.5 M; 1 M; 2 M; 3 M) dissolved in TMP.

Synthesis of PTMA-10%C

The synthesis was carried out as reported elsewhere.[1] This material has been used for all PTMA-based electrodes.

PTMA electrodes used for studies of phosphate concentration effect

600 mg Of PTMA-10%C composite were mixed with 250 mg of SC45 and thoroughly grinded. To this mixture, 50 mg of SBR (dissolved in water, 5 wt.%) and 100 mg of CMC (dissolved in water at a concentration of 2 - 4 wt.%) were added and thoroughly stirred. The obtained slurry was coated on carbon coated aluminum foil followed by drying in air at 50 °C. Disks of 0.5 in diameter (loading around 5 mg/cm^2)

were subsequently punched and pressed at 6 tons/cm^2. Prior the cell assembly, the electrodes were dried at 55 °C in vacuum for 12 h.

The electrodes were tested in half-cell configuration using Li-metal foil as reference and counter electrode. CR2032 coin-cells were used. One sheet of Celgard separator was placed in between the working electrode and lithium disk. The cells were activated by soaking the electrodes and the separator with the electrolyte solution. The electrolyte solution was prepared by mixing EC/DEC 1 M $LiPF_6$ commercial electrolyte, adding either TEP or TMP, and $LiPF_6$ to adjust the final lithium salt concentration to be equal to 1 M. The cells were assembled in an argon-filled glove box.

PTMA-based hybrid electrodes preparation

Same procedure as described beforehand for all-PTMA slurry preparation and coin-cell assembly was applied for hybrid electrodes with the following compositions (weight ratios): PTMA-10%C / LFP / SC45 / CMC / SBR 40:20:25:10:5. These cells were tested in cyclic voltammetry experiments using either EC/DEC/TMP 25:25:50 (v:v:v) 1 M $LiPF_6$ or EC/DEC 50:50 (v/v) 1 M $LiPF_6$. (scan rate = 0.2 mV.s^{-1})

Cell design of $Li_4Ti_5O_{12}$-PTMA dual-ions batteries

LTO anode. Slurry preparation from LTO, SC45 and PVDF (80:10:10 w/w/w) through ball-milling of the constituents (400 rpm, 45 min). The slurry was spread on carbon coated Al foil by means of the doctor blade method. The wet film thicknesses were adjusted to 500 µm (loadings around 3.0 mg/cm²). The coated foil was then cut into discs (diameter, 0.5 in, coating mass around 8.0 mg each).

PTMA cathode. Self-standing electrodes were produced using a vacuum filtration process over a PVDF 0.2 µm filter. The filtration device is a Millipore set-up. Pristine MWCNTs (6.25 mg) were dispersed in butanol (200 mL) using bath sonication for 30 min. This first suspension was filtered on the PVDF filter. A suspension of PTMA/10%C (25 mg) and pristine MWCNTs (6.25 mg) was then prepared in BuOH (400 mL, bath sonicated for 30 min) and filtered over the first layer formed on PVDF (3.40 cm diameter). Electrodes were first dried in ambient air at room temperature for 2 hours, then at 60°C under vacuum for 24 hours. The resulting buckypaper was then cut into discs (diameter, 0.5 in, mass around 7.5 mg each).

Cell assembly. The electrodes were assembled in a CR2025 case, using Celgard separator, in a glovebox under argon, using either EC/DEC 1 M $LiPF_6$, or TMP 1 M $LiPF_6$ as electrolyte.

Electrochemical testing. Galvanostatic cycling was carried out at C-rate equal to C/5 with respect to the LTO electrode capacity.

Electrolyte stability window

The electrolyte anodic stability was obtained in a CR2032 coin cell assembled in an Ar filled glovebox, using Li as WE and pseudo-RE, carbon-coated Al foil as CE and Celgard as separator. The electrolyte was either TMP 1 M $LiPF_6$ or either EC/DEC 1 M $LiPF_6$ and cyclic voltammetry experiments were carried out at 1 mV.s^{-1}.

Voltage shifts with other phosphorus-based derivatives

These experiments are relying on the same procedure designed to study the phosphate concentration effect. The electrolytes used here have the following composition: EC / DEC / Pi 25:25:50 (v/v/v) 1 M $LiPF_6$, where Pi is one of the following compounds, TBP, TMPOx, TMThP.

Na based systems

This experiment was carried in a glovebox under argon. A beaker cell was loaded with the electrolyte solution, TMP 1M $NaPF_6$. The first test involved the following set of electrodes: a Ni disc as WE, a sodium chip stuck on a copper support as CE, Ag/AgCl in presence of NBu_4Cl (0.004 M) as pseudo-RE electrode. Ferrocene (2 mg/mL) was added to the electrolyte medium as reference electrochemical system (RES). An anodic polarization was carried out and ferrocene redox response was recorded at 50 $mV.s^{-1}$ both versus the Na^+/Na CE and the Ag/AgCl pseudo-RE.

Instrumentation

Cyclic voltammetry. All experiments have been carried out under an argon atmosphere (<0.1 ppm H_2O, <0.1 ppm O_2) in a glovebox from Innovative Technology, Inc., using a PARTSTAT 3000 potentiostat from Princeton Applied Research.

2. Electrochemical Data.

Figure S1.

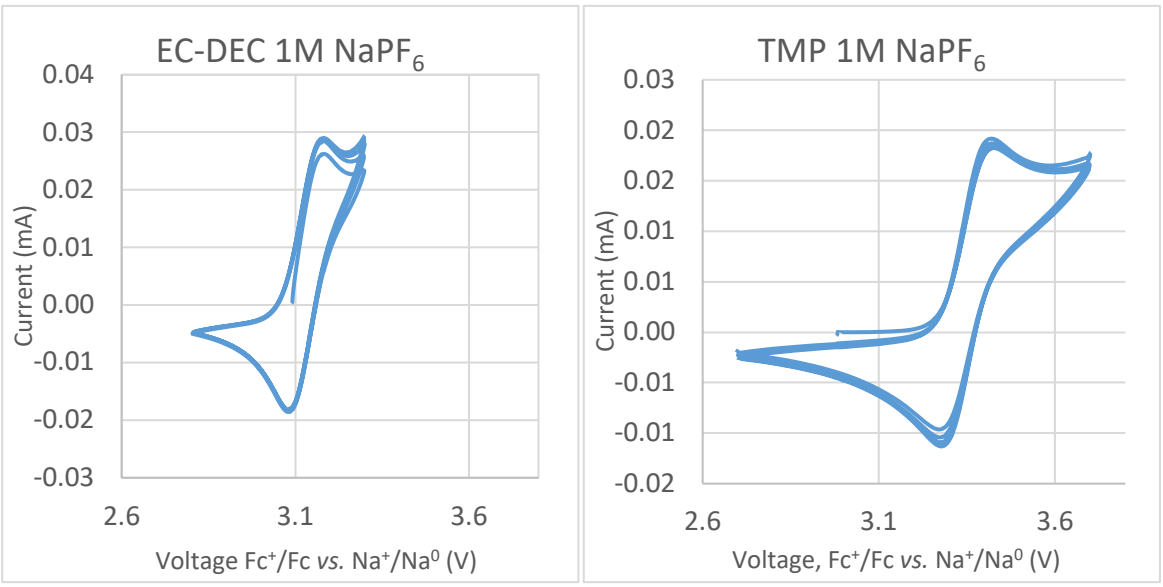

	$E_{1/2}$ (V) vs Na^+/Na
EC/DEC	***3.13***
TMP	***3.34***

In this set of experiments, we highlight the effect of phosphates on the redox potential of the Na^+/Na^0 couple, which is found to be significantly affected in a similar manner as for the Li^+/Li^0 redox couple. To this end we compare the voltage difference obtained between a Na^+/Na^0 electrode and the redox response of the reference electrochemical system Fc^+/Fc. The redox shift measured in these conditions was found to be of ca. 210 mV.

Figure S2.

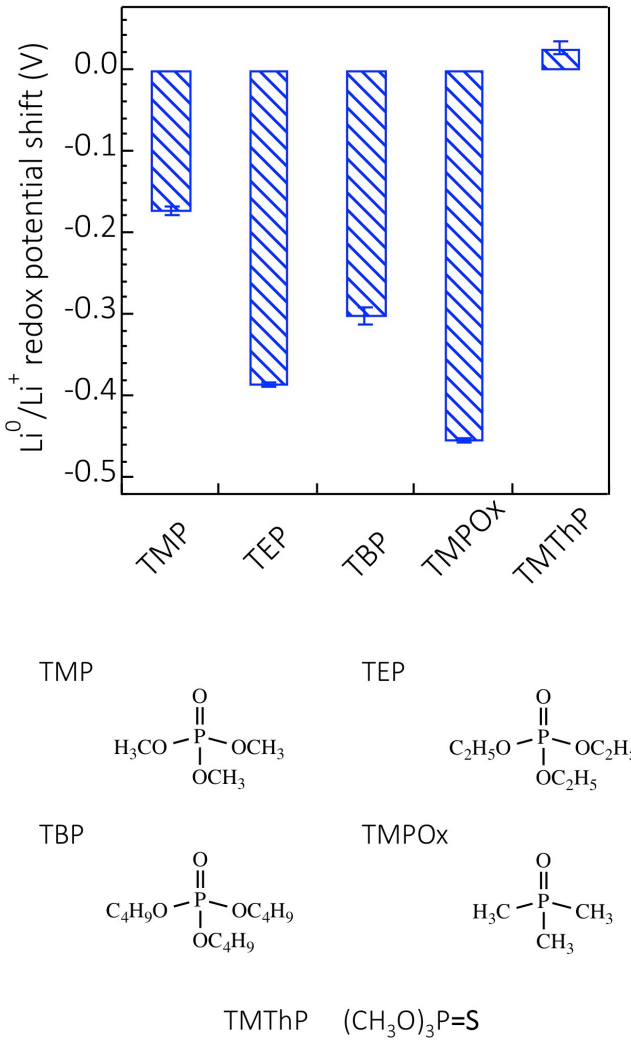

Redox potential shift with other phosphates. All data are obtained at a concentration of 3.68 M phosphate in the ternary EC/DEC/Phosphate system, all at 1 M Lithium salt.

Table S1. Composition and molar ratio of the ternary systems presented in Fig. 2.

TMP/Li molar ratio	vol%_TMP	vol%_EC	vol%/DEC	Li molar	TMP/Li molar ratio	EC/Li molar ratio	DEC/Li molar ratio	TMP/(EC+DEC) molar ratio	Solvent to Li molar ratio
0	0	50	50	1	0.0	7.5	4.1	0.0	11.6
0.85	10	45	45	1	0.9	6.7	3.7	0.1	11.3
2.14	25	37.5	37.5	1	2.1	5.6	3.1	0.2	10.9
3.16	37.5	31.25	31.25	1	3.2	4.7	2.6	0.4	10.4
4.27	50	25	25	1	4.3	3.7	2.1	0.7	10.1
5.13	60	20	20	1	5.1	3.0	1.7	1.1	9.8
6.41	75	12.5	12.5	1	6.4	1.9	1.0	2.2	9.3
8.55	100	0	0	1	8.6	0	0	---	8.6

TEP/Li molar ratio	vol%_TEP	vol%_EC	vol%/DEC	Li molar	TEP/Li molar ratio	EC/Li molar ratio	DEC/Li molar ratio	TEP/(EC+DEC) molar ratio	Solvent to Li molar ratio
0	0	50	50	1	0	7.5	4.1	0.0	11.6
0.59	10	45	45	1	0.59	6.7	3.7	0.1	11.0
1.47	25	37.5	37.5	1	1.47	5.6	3.1	0.2	10.2
2.17	37	31.25	31.25	1	2.17	4.7	2.6	0.3	9.4
2.94	50	25	25	1	2.94	3.7	2.1	0.5	8.8
3.52	60	20	20	1	3.52	3.0	1.7	0.8	8.2
4.41	75	12.5	12.5	1	4.41	1.9	1.0	1.5	7.3
5.87	100	0	0	1	5.87	0	0	---	5.9

Figure S3.

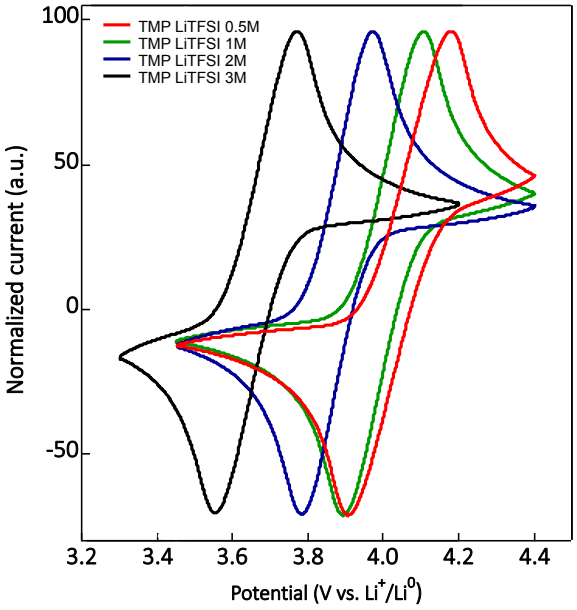

Tempo redox response recorded in TMP based electrolytes against a Li/Li^+ electrode. The concentration of the lithium salt is varying from 0.5 M to 3 M. This set of CV experiments evidences the influence of Li salt concentration on Li^+/Li redox potential in TMP based electrolytes. According to Nernst equation, the effect on the measured voltage difference between the Tempo redox couple and the Li^+/Li^0 should affect both electrodes symmetrically: (i) Due to the increase of the counter-anion concentration ($TFSI^-$), Tempo should be shifted towards lower values by a factor of 59 mV per concentration decade;[2] (ii) the Li electrode should be affected the same way, 59 mV per decade, due to the increase of the Li+ concentration of the system;[3] (iii) these two effects should be cancelling out each other on the resulting voltage. Yet a much important difference (about 410 mV) is observed between the lowest and highest electrolyte concentration (respectively 0.5 and 3 M), which is due to deviations from Nernst equation. The deviation from Nernst should be related to the high concentration regime of the measurements and is ascribed to the change of the activities of $Li(TMP)_n^+$ complex and free solvent.

Li/Molarity	TMP-to-Li molar ratio
0.5	17.1
1	8.6
2	4.3
3	2.9

3. NMR experiments

A series of electrolyte solutions were prepared in an argon atmosphere glovebox by dissolving 1 mol dm^{-1} $LiPF_6$ or LiTFSI in a mixture of EC\DEC\TMP or EC\DMC\TMP (1:1:*x*, v:v:v %), respectively. Percentage of TMP ranges from 0 (EC\DEC\TMP or EC\DMC\TMP 1:1:0 v:v:v) to 100 (EC\DEC\TMP or EC\DMC\TPM 0:0:1 v:v:v), passing by 10%, 25%, 37.5%, 50%, 60% and 75% (as reported in the Table S1). Toluene (Sigma-Aldrich, anhydrous, aliquots of 25 µL to each NMR tube) was added as internal standard for DOSY NMR analyses. Moreover, in DOSY NMR analyses some of these solutions have been compared with the corresponding unsalted electrolyte mixtures.

Neat samples of these solutions were analyzed by NMR spectroscopy using standard 5 mm thin-walled tubes with coaxial NMR inserts (0.15 mL of C_6D_6 (Eurisotop) therein) placed inside the NMR tubes. All ^{1}H, ^{7}Li, ^{13}C, and ^{31}P NMR spectra were recorded at room temperature (296 K) on a Bruker Avance 500 spectrometer operating at 500.13 MHz, 194.37 MHz, 125.76 MHz and 202.46 MHz, respectively. Experiments were run using a BBO{1H,X} probehead equipped with a *z*-gradient coil, allowing a maximum gradient strength of 0.5 T/m. The ^{1}H and ^{13}C resonances were referenced to C_6D_6 (7.16 ppm for ^{1}H and 128.06 ppm for ^{13}C NMR spectra). ^{31}P and ^{7}Li NMR spectra were calibrated using external references: a 85% H_3PO_3 solution in H_2O (δ = 0.00 ppm) for ^{31}P NMR spectra and 1.0 M $^{7}LiCl$ solution in D_2O for ^{7}Li NMR experiments. Standard zg programs were employed for 1D NMR experiments. A Waltz-16 decoupling scheme with a pulse of 80 µsec was used for $^{13}C\{^{1}H\}$ and $^{31}P\{^{1}H\}$ NMR analyses. ^{1}H DOSY measurements were performed using the standard Bruker ledbpgp2s pulse program with 16 t1 increments on 32 K data points. Acquisition times were fixed to 4.2 s, 2.0 s and 0.65 s for ^{1}H, ^{7}Li and ^{31}P, respectively, and relaxation delays (D1) ranged from 2 s (^{7}Li and ^{31}P) to 30 s (^{1}H). Diffusion times (D20) of 0.5 s (^{1}H) and 1.0 s (^{7}Li and ^{31}P) and rectangular gradient pulse durations (P30) of 0.8 ms, 2 ms and 3.0 ms were applied for ^{1}H, ^{7}Li and ^{31}P, respectively. Gradient recovery delays between 0.15 (^{1}H) and 0.5 ms (^{7}Li and ^{31}P) followed the application of each gradient pulse. Data were accumulated by linearly varying the diffusion encoding gradients over a range from 2 to 95 % for 16 gradient increment values. Individual rows of the quasi-2D diffusion databases were phased and baseline corrected. Processing of NMR data were performed using Topspin software (by Bruker supplier), and the actual diffusion coefficients used for diffusion analysis were measured by T_1/T_2 relaxation module.

[1]H, [7]Li and [31]P NMR chemical shift analysis

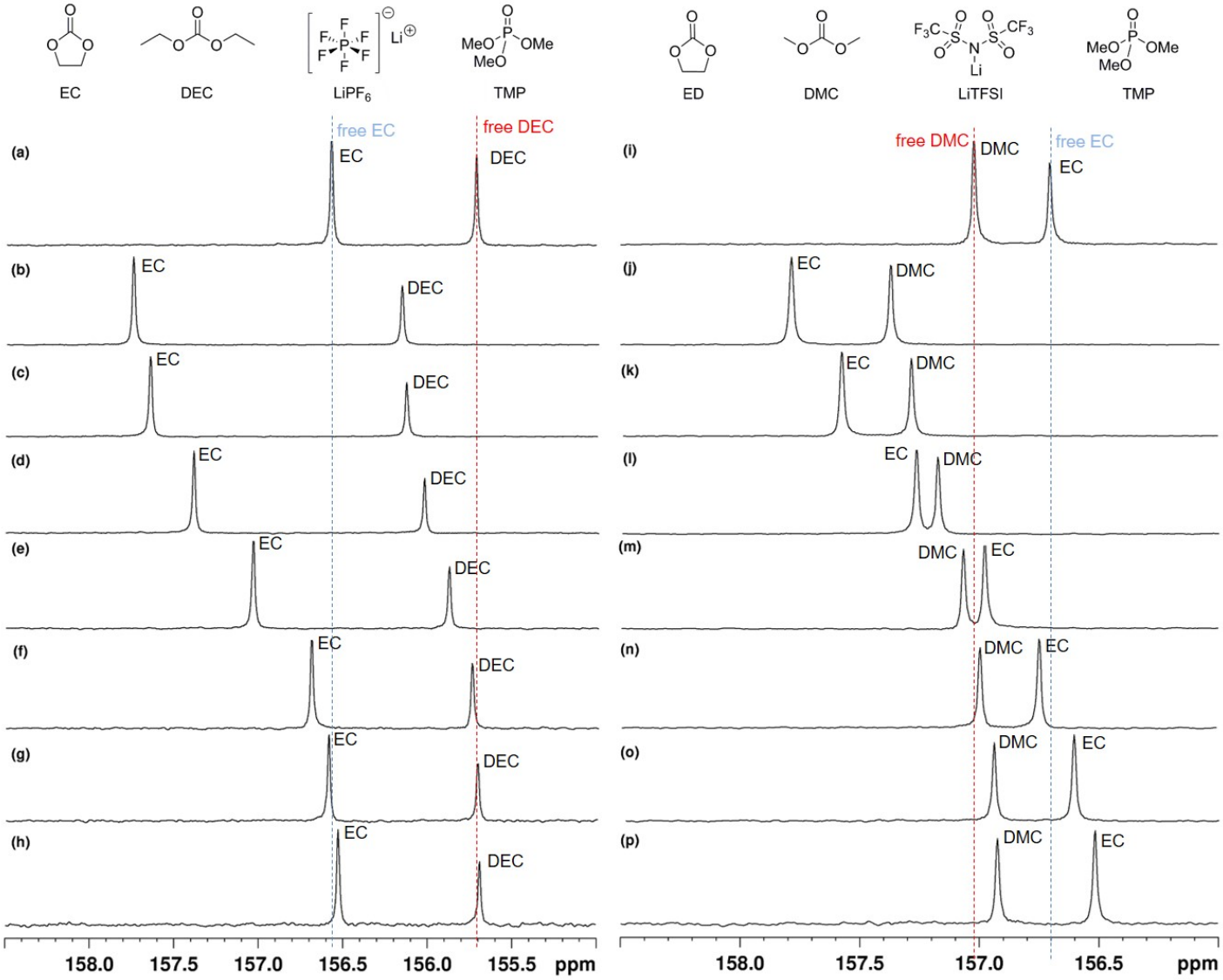

Figure S4. $^{13}C\{^{1}H\}$ NMR spectra. Left: (a) EC + DEC, (b) EC + DEC + $LiPF_6$, (c) EC + DMC + $LiPF_6$ + (10%) TMP, (d) EC + DEC + $LiPF_6$ + (25%) TMP, (e) EC + DEC + $LiPF_6$ + (37.5%) TMP, (f) EC + DEC + $LiPF_6$ + (50%) TMP, (g) EC + DEC + $LiPF_6$ + (60%) TMP, (h) EC + DEC + $LiPF_6$ + (75%) TMP. Right: (i) EC + DMC, (j) EC + DMC + LiTFSI, (k) EC + DMC + LiTFSI + (10%) TMP, (l) EC + DMC + LiTFSI + (25%) TMP, (m) EC + DMC + LiTFSI + (37.5%) TMP, (n) EC + DMC + LiTFSI + (50%) TMP, (o) EC + DMC + LiTFSI + (60%) TMP, (p) EC + DMC + LiTFSI + (75%) TMP. The spectra are restricted to the 160.0 ppm ÷ 155.0 ppm zone. Note that, on the spectra on the right, NMR chemical shifts of "free" DMC/EC in (i) and the "supposed" to be "free DMC/EC species" in (n-p) don't line up well probably because of a different viscosity of the solutions.

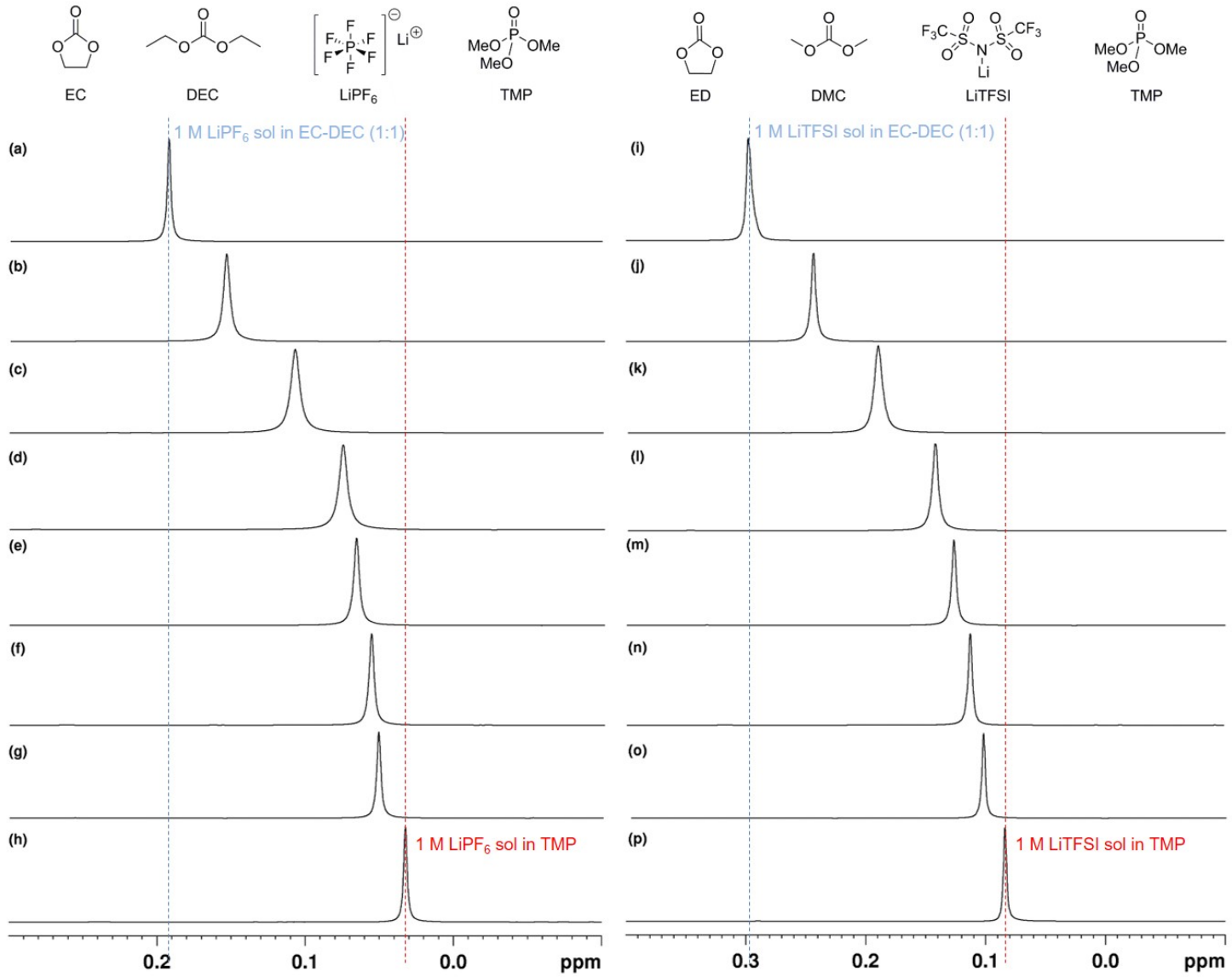

Figure S5. ^{7}Li NMR spectra. Left: (a) EC + DEC + $LiPF_6$, (b) EC + DMC + $LiPF_6$ + (10%) TMP, (c) EC + DEC + $LiPF_6$ + (25%) TMP, (d) EC + DEC + $LiPF_6$ + (37.5%) TMP, (e) EC + DEC + $LiPF_6$ + (50%) TMP, (f) EC + DEC + $LiPF_6$ + (60%) TMP, (g) EC + DEC + $LiPF_6$ + (75%) TMP, (h) $LiPF_6$ + TMP. Right: (i) EC + DMC + LiTFSI, (j) EC + DMC + LiTFSI + (10%) TMP, (k) EC + DMC + LiTFSI + (25%) TMP, (l) EC + DMC + LiTFSI + (37.5%) TMP, (m) EC + DMC + LiTFSI + (50%) TMP, (n) EC + DMC + LiTFSI + (60%) TMP, (o) EC + DMC + LiTFSI + (75%) TMP (p) LiTFSI + TMP.

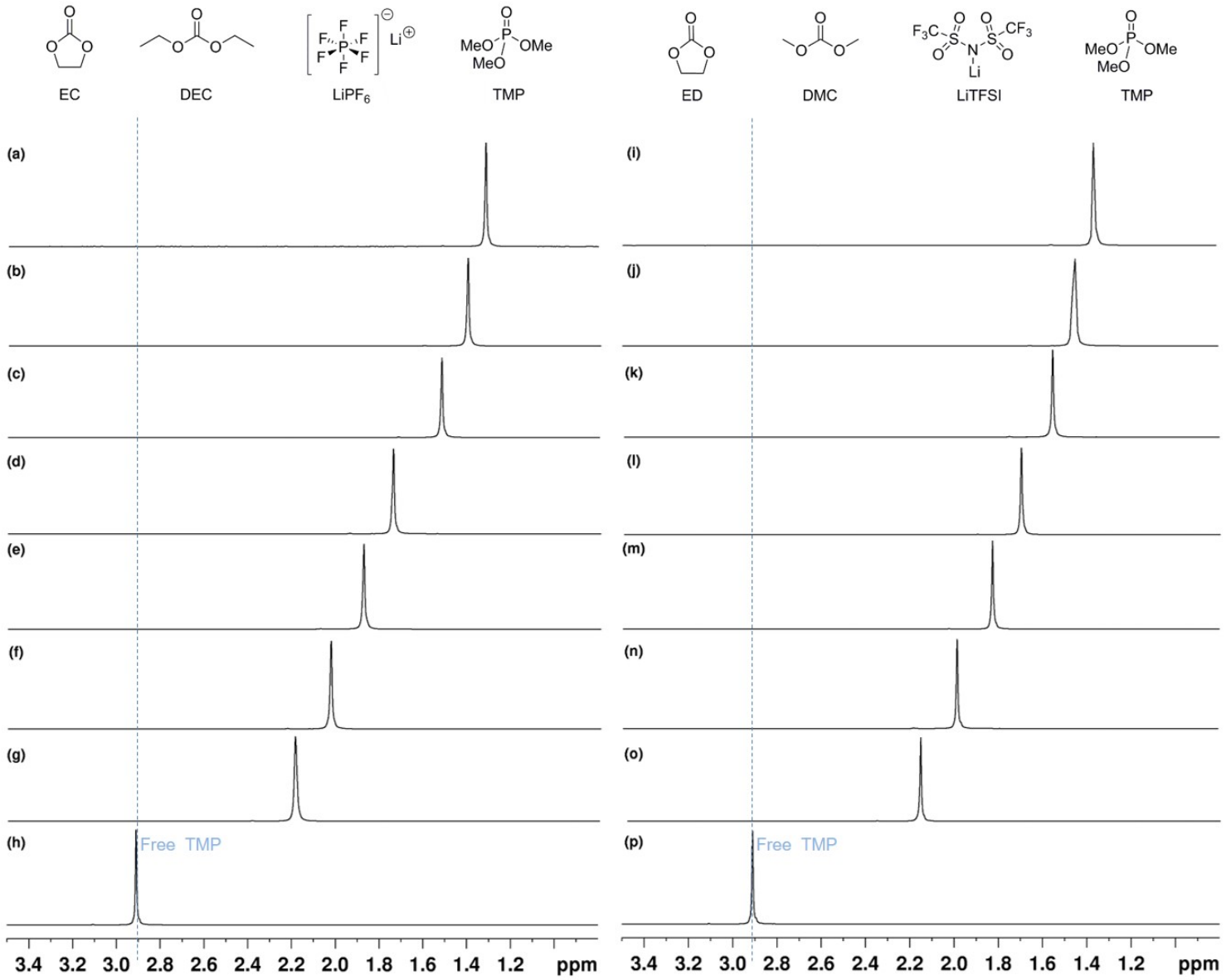

Figure S6. $^{31}P\{^{1}H\}$ NMR spectra. Left (a) EC + DMC + $LiPF_6$ + (10%) TMP, (b) EC + DEC + $LiPF_6$ + (25%) TMP, (c) EC + DEC + $LiPF_6$ + (37.5%) TMP, (d) EC + DEC + $LiPF_6$ + (50%) TMP, (e) EC + DEC + $LiPF_6$ + (60%) TMP, (f) EC + DEC + $LiPF_6$ + (75%) TMP, (g) $LiPF_6$ + TMP, (h) TMP. Right: (i) EC + DMC + LiTFSI + (10%) TMP, (j) EC + DMC + LiTFSI + (25%) TMP, (k) EC + DMC + LiTFSI + (37.5%) TMP, (l) EC + DMC + LiTFSI + (50%) TMP, (m) EC + DMC + LiTFSI + (60%) TMP, (n) EC + DMC + LiTFSI + (75%) TMP, (o) LiTFSI + TMP, (p) TMP.

^{1}H, ^{7}Li and ^{31}P DOSY and diffusion coefficient (Diff.) analysis

Table S2. Experimental diffusion coefficient (10^{-10} m^2 s^{-1}) data.

Solutions	**Composition[(a)]**	**$^{1}H_{Tol}$ Diff.[(b)]**	**$^{1}H_{DEC(CH2)}$ Diff.[(b)]**	**$^{1}H_{EC}$ Diff.[(b)]**	**$^{1}H_{TMP}$ Diff.[(b)]**	**$^{31}P_{TMP}$ Diff.[(b)]**	**^{7}Li Diff.[(b)]**
A : EC + DEC	1:1	11.01	9.14	9.62	n/a	n/a	n/a
B : EC + DEC + $LiPF_6$	7.5:4.1:1	5.96	7.21	3.75	n/a	n/a	1.73
C : : (25%) TMP + EC + DEC	1:1.5:1,5	10.26	8.32	8.96	7.46	1.27	n/a
D : (25%) TMP + EC + DEC + $LiPF_6$	2.1:5.6:3.1: 1	6.28	7.81	4.57	3.43	0.28	1.81
E : (50%) TMP + EC + DEC	1.5:1:1	10.02	8.20	8.78	7.24	1.21	n/a
F : (50%) TMP + EC + DEC + $LiPF_6$	4.2:3.7:2.1:1	6.33	8.81	5.34	4.05	0.42	2.15
G : (75%) TMP + EC + DEC	6:1:1	9.24	7.78	8.22	6.74	1.11	n/a
H : (75%) TMP + EC + DEC + $LiPF_6$	6.4:1.9:1:1	4.72	8.71	4.02	4.94	0.34	1.60
I : TMP	1	9.18	n/a	n/a	8.38	1.17	n/a
J : (100%) TMP + $LiPF_6$	8.5:1	5.10	n/a	n/a	5.49	0.43	1.48

[(a)]: Determined by considering the molar ratios in a 1 M $LiPF_6$ (or unsalted) solution prepared from a mixture of TMP+EC+DEC (v:v:v%, where v = volume) (see Table S1);
[(b)]: ^{1}H Diffusion Coefficients have been extrapolated from ^{1}H DOSY measures and reported in units of 10^{-10} m^2/s.

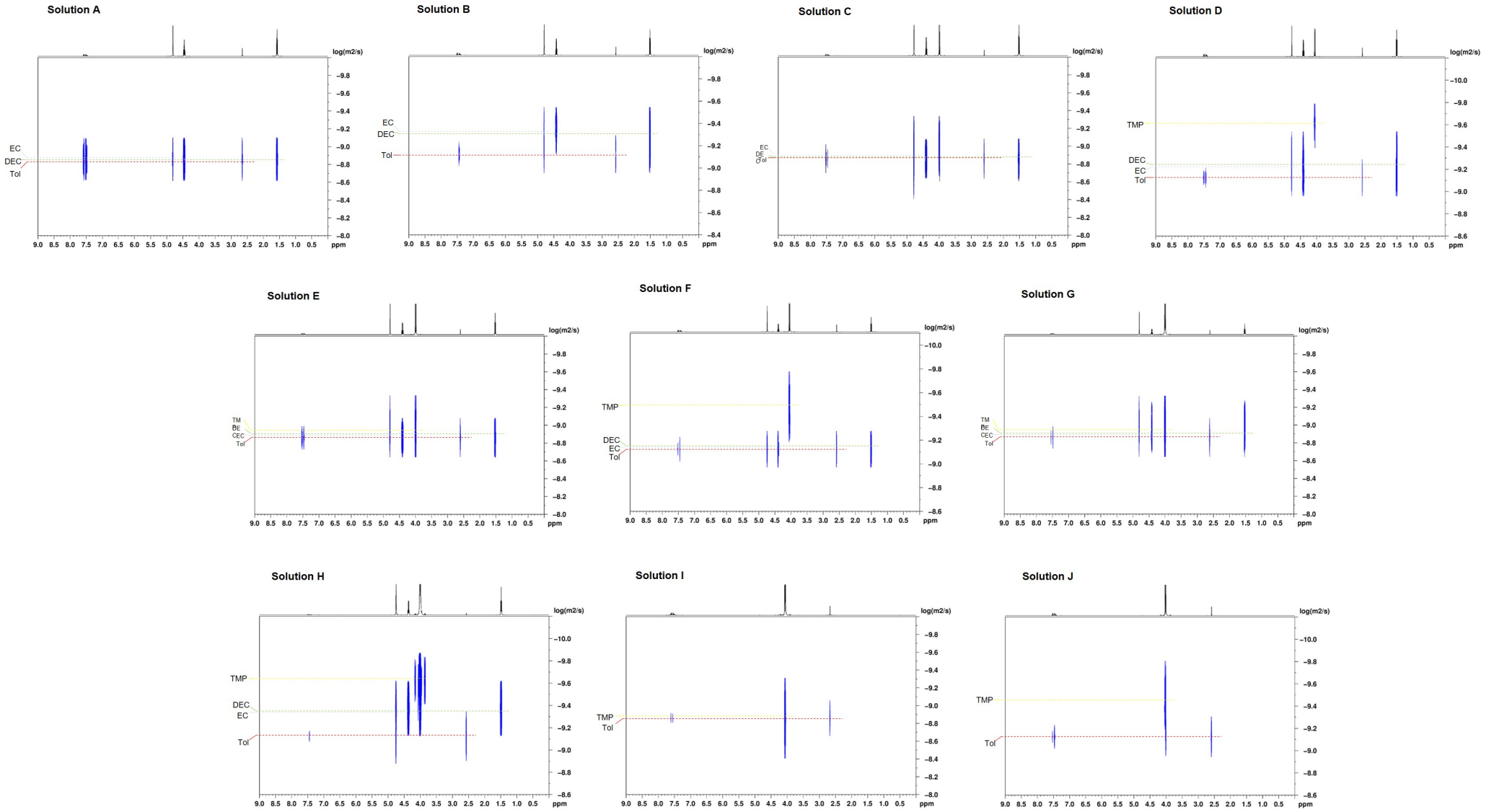

Figure S7. ^{1}H DOSY NMR spectra of A-J solutions. (A): EC + DMC, (B): EC + DMC + $LiPF_6$, (C): EC + DEC + (25%) TMP, (D): EC + DEC + $LiPF_6$ + (25%) TMP, (E): EC + DEC + (50%) TMP, (F): EC + DEC + $LiPF_6$ + (50%) TMP, (G): EC + DEC + (75%) TMP, (H): EC + DEC + $LiPF_6$ + (75%) TMP, (I): TMP, (J): $LiPF_6$ + TMP.

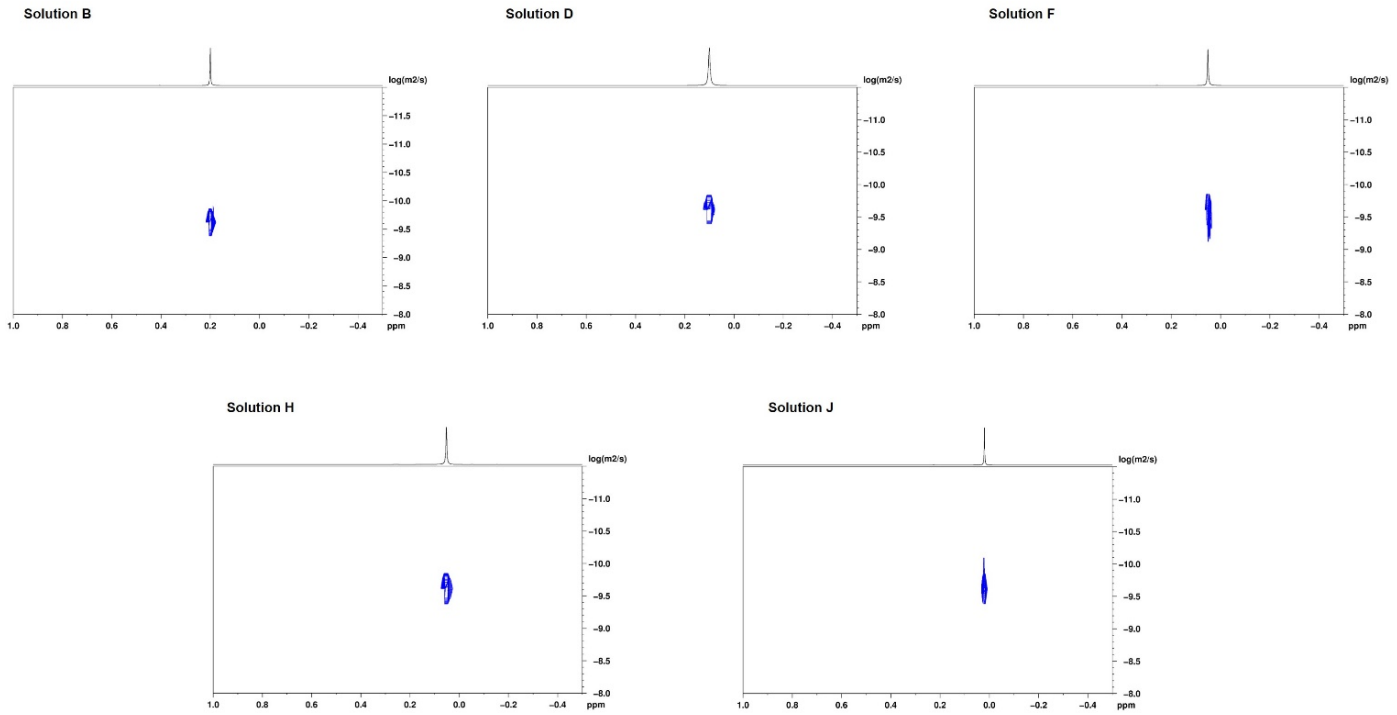

Figure S8. ^{7}Li DOSY NMR spectra of the following solutions: (B) EC + DMC + $LiPF_6$, (D) EC + DEC + $LiPF_6$ + (25%) TMP, (F: EC + DEC + $LiPF_6$ + (50%) TMP, (H) EC + DEC + $LiPF_6$ + (75%) TMP, (J) $LiPF_6$ + TMP.

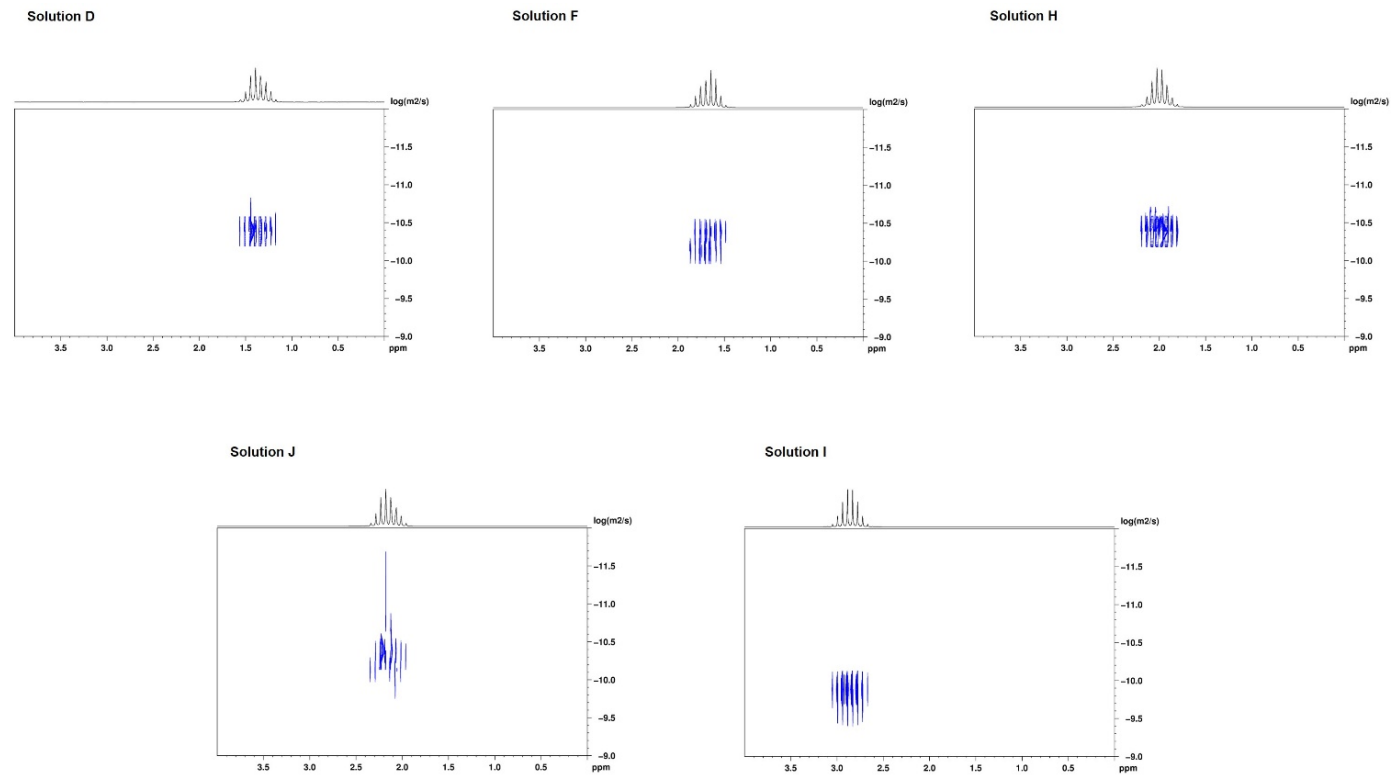

Figure S9. ^{31}P DOSY NMR spectra of the following solutions: (D) EC + DEC + $LiPF_6$ + (25%) TMP, (F) EC + DEC + $LiPF_6$ + (50%) TMP, (H) EC + DEC + $LiPF_6$ + (75%) TMP, (J) $LiPF_6$ + TMP, (I) TMP.

4. ^{1}H, ^{7}Li and ^{31}P DOSY corrections

Table S3. ^{1}H Diffusion coefficients (10^{-10} m^2 s^{-1}) after corrections.

Solutions	$^{1}H_{Tol}$ Diff.[a]	Δ[b]	$^{1}H_{Tol}$ [Diff.][c]	$^{1}H_{EC}$ Diff.[a]	$^{1}H_{EC}$ [Diff.][c]	$^{1}H_{DEC(CH2)}$ Diff.[a]	$^{1}H_{DEC(CH2)}$ [Diff.][c]	$^{1}H_{TMP}$ Diff.[a]	$^{1}H_{TMP}$ [Diff.][c]
A : EC + DEC	11.01	1	11.01	9.62	9.62	9.14	9.14	n/a	n/a
B : EC + DEC + $LiPF_6$	5.96	1.85	11.01	3.75	6.92	3.90	7.21	n/a	n/a
D : (25%) TMP + EC + DEC + $LiPF_6$	6.28	1.75	11.01	4.57	8.01	4.45	7.81	1.96	3.43
D : (50%) TMP + EC + DEC + $LiPF_6$	6.33	1.74	11.01	5.34	9.29	5.07	8.81	2.33	4.05
H : (75%) TMP + EC + DEC + $LiPF_6$	4.72	2.33	11.01	4.02	9.38	3.73	8.71	2.12	4.94
J : (100%) TMP + $LiPF_6$	5.10	2.16	11.01	n/a	n/a	n/a	n/a	2.54	5.49
I : TMP	9.18	1.20	11.01	n/a	n/a	n/a	n/a	6.98	8.38

[a]: Experimental ^{1}H Diffusion Coefficients from DOSY measurements;
[b]: Correction factor; determined by ^{1}H NMR DOSY experiments according to equation 2 (see Supplementary Paragraph 6)
[c]: ^{1}H Diffusion Coefficients after corrections.

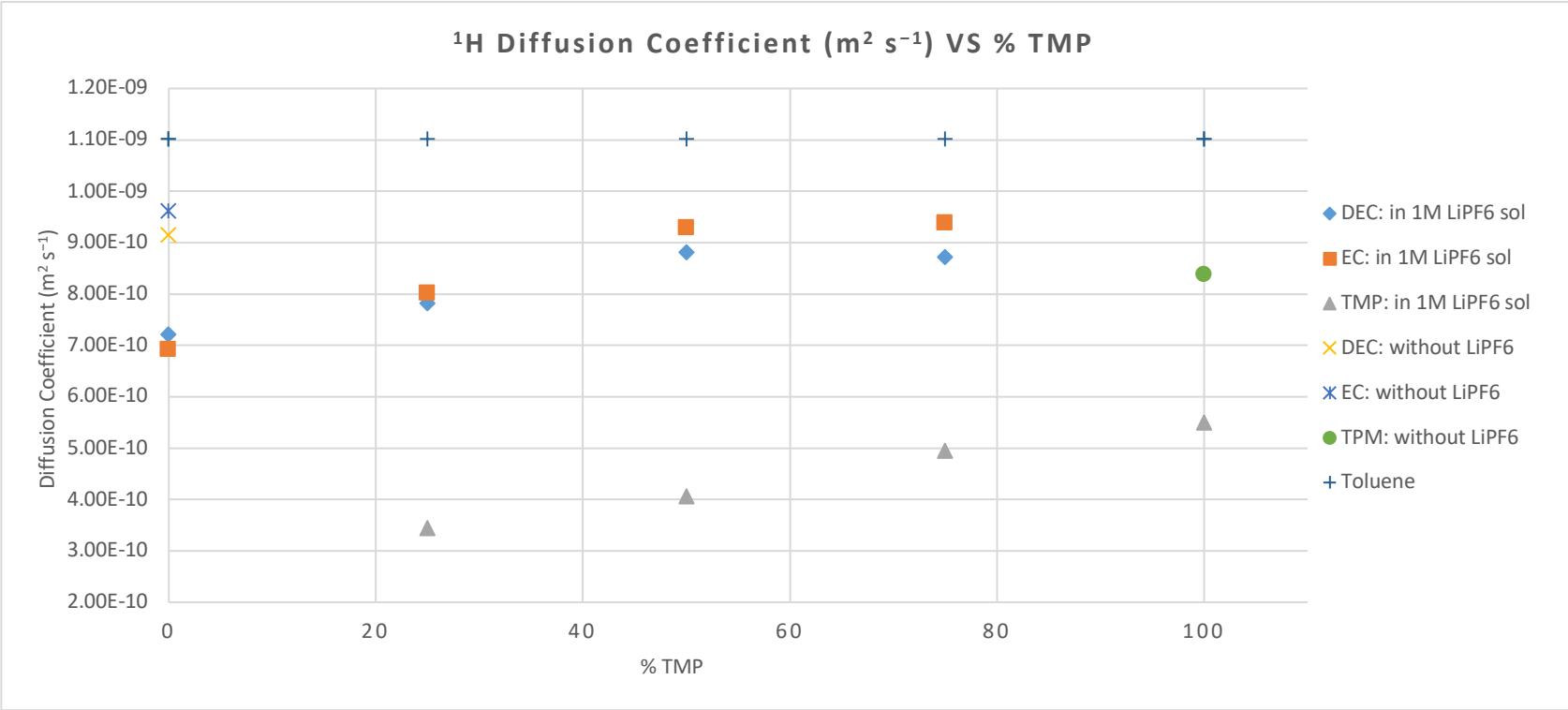

Table S4. ^{7}Li Diffusion coefficients (10^{-10} m^2 s^{-1}) after corrections.

Solutions	Δ[(a)]	^{7}Li Diff.[(b)]	^{7}Li [Diff.][(c)]
A : EC + DEC	1	n/a	n/a
B : EC + DEC + $LiPF_6$	1.85	1.73	3.21
D : (25%) TMP + EC + DEC + $LiPF_6$	1.75	1.81	3.17
D : (50%) TMP + EC + DEC + $LiPF_6$	1.74	2.15	3.74
H : (75%) TMP + EC + DEC + $LiPF_6$	2.33	1.60	3.74
J : (100%) TMP + $LiPF_6$	2.16	1.48	3.19
I : TMP	1.20	n/a	n/a

[(a)]: Correction factor; determined by ^{1}H NMR DOSY experiments according to equation 2 (see Supplementary Paragraph 6);
[(b)]: Experimental ^{1}H Diffusion Coefficients from DOSY measurements;
[(c)]: ^{1}H Diffusion Coefficients after corrections.

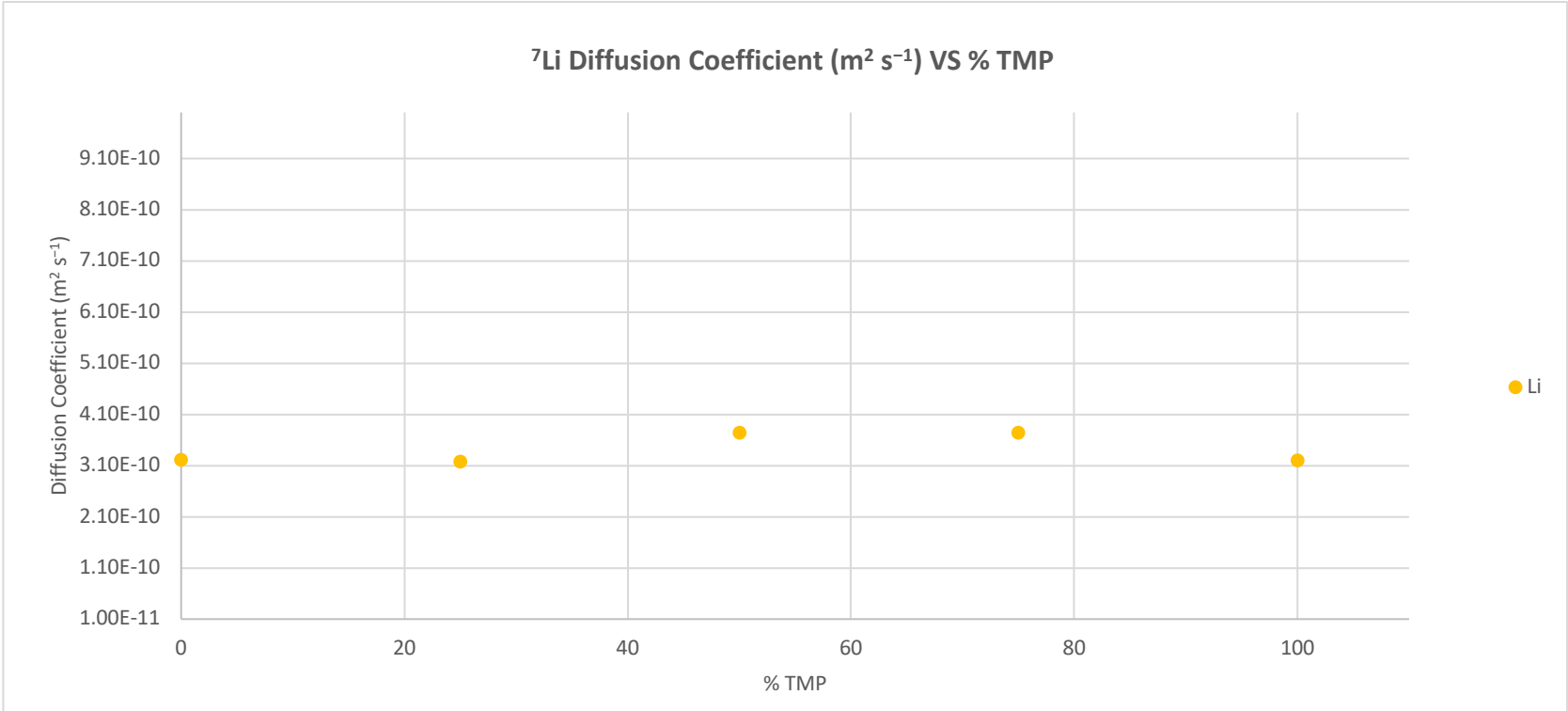

Table S5. ^{31}P Diffusion coefficients (10^{-10} m^2 s^{-1}) after corrections.

Solutions	$\Delta^{(a)}$	$^{31}P_{TMP}$ Diff.$^{(b)}$	$^{31}P_{TMP}$ [Diff.]$^{(c)}$
A : EC + DEC	1	n/a	n/a
B : EC + DEC + $LiPF_6$	1.85	n/a	n/a
D : (25%) TMP + EC + DEC + $LiPF_6$	1.75	0.28	0.50
D : (50%) TMP + EC + DEC + $LiPF_6$	1.74	0.42	0.73
H : (75%) TMP + EC + DEC + $LiPF_6$	2.33	0.34	0.80
J : (100%) TMP + $LiPF_6$	2.16	0.43	0.93
I : TMP	1.20	1.17	1.41

(a): Correction factor; determined by ^1H NMR DOSY experiments according to equation 2 (see Supplementary Paragraph 6);
(b): Experimental ^1H Diffusion Coefficients from DOSY measurements;
(c): ^1H Diffusion Coefficients after corrections.

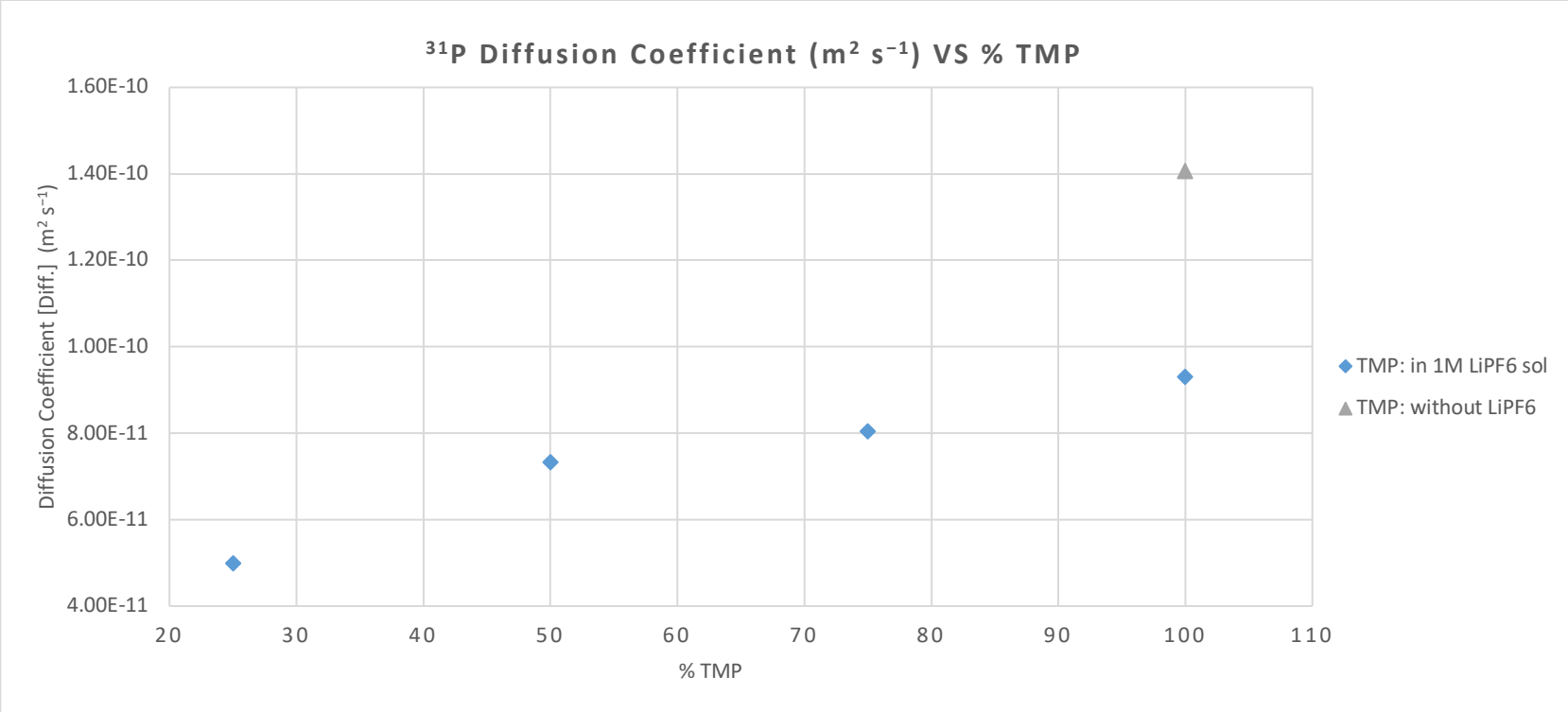

5. Coordination ratio "α" and coordination number of lithium by DOSY NMR experiments

Table S6. Coordination ratio α of electrolytes EC, DEC and TMP in the solutions A to J.

Solutions	**Composition**[a]	**^{1}H D_{Tol}**[b]	**^{1}H D_{EC}**[b]	**^{1}H $D_{DEC(CH2)}$**[b]	**^{1}H$_{TMP}$**[b]	**^{7}Li D**[b]	**α_{EC}**[c]	**α_{DEC}**[c]	**α_{TMP}**[c]
A : EC:DEC	1:1	11.01	9.62	9.14	n/a	n/a			
B : EC:DEC:$LiPF_6$	7.5:4.1:1	5.96	3.75	7.21	n/a	1.73	0.42 ± 0.01	0.33 ± 0.01	n/a
C : 25%TMP:EC:DEC	1:1.5:1.5	10.26	8.96	8.32	7.46	n/a			
D : 25%TMP:EC:DEC:$LiPF_6$	2.1:5.6:3.1: 1	6.28	4.57	7.81	3.43	1.81	0.25 ± 0.01	0.19 ± 0.01	0.95 ± 0.01
E : 50%TMP:EC:DEC	1.5:1:1	10.02	8.78	8.20	7.24	n/a			
F : 50%TMP:EC:DEC:$LiPF_6$	4.2:3.7:2.1:1	6.33	5.34	8.81	4.05	2.15	0.06 ± 0.01	0.04 ± 0.01	0.92 ± 0.01
G : 75%TMP:EC:DEC	6:1:1	9.24	8.22	7.78	6.74	n/a			
H : 75%TMP:EC:DEC:$LiPF_6$	6.4:1.9:1:1	4.72	4.02	8.71	4.94	1.60	0.07 ± 0.01	0.10 ± 0.01	0.72 ± 0.01
I : 100%TMP	1	9.18	n/a	n/a	8.38	n/a			
J : 100%TMP:$LiPF_6$	8.5:1	5.10	n/a	n/a	5.49	1.48	n/a	n/a	0.56 ± 0.01

[a]: Determined by considering the molar ratios in a 1 M $LiPF_6$ (or unsalted) solution prepared from a mixture of TMP+EC+DEC (v:v:v%, where v = volume) (see Table S1);
[b]: ^{1}H Diffusion Coefficients have been extrapolated from ^{1}H DOSY measures and reported in units of 10^{-10} m^2/s;
[c]: The errors were calculated considering the 2% typical inaccuracy limit of the diffusion NMR techniques.

Table S7. Coordination number of Li in the solutions A to J.

Solutions	**Composition[a]**	**Coordination Number of Li[b]**	**%Li coordinated with TMP[c]**	**%Li coordinated with EC[c]**	**%Li coordinated with DEC[c]**	**structures presupposed $Li(DEC/EC)_x(TMP/TEP)_y$**
A : EC:DEC	1:1					n/a
B : EC:DEC:$LiPF_6$	7.5:4.1:1	4.5 ± 0.1	0	69.95	30.05	$Li(DEC/EC)_4(TMP/TEP)_0$
C : 25%TMP:EC:DEC	1:1.5:1.5					n/a
D : 25%TMP:EC:DEC:$LiPF_6$	2.1:5.6:3.1: 1	4.0 ± 0.1	50.07	35.15	14.78	$Li(DEC/EC)_2(TMP/TEP)_2$
E : 50%TMP:EC:DEC	1.5:1:1					n/a
F : 50%TMP:EC:DEC:$LiPF_6$	4.2:3.7:2.1:1	4.2 ± 0.1	92.66	5.32	2.02	$Li(DEC/EC)_{\approx 0}(TMP/TEP)_{\approx 4}$
G : 75%TMP:EC:DEC	6:1:1					n/a
H : 75%TMP:EC:DEC:$LiPF_6$	6.4:1.9:1:1	4.8 ± 0.1	95.19	2.75	2.06	$Li(DEC/EC)_{\approx 0}(TMP/TEP)_{\approx 4}$
I : 100%TMP	1					n/a
J : 100%TMP:$LiPF_6$	8.5:1	4.8 ± 0.1	100	0	0	$Li(DEC/EC)_0(TMP/TEP)_4$

[a]: Determined by considering the molar ratios in a 1 M $LiPF_6$ (or unsalted) solution prepared from a mixture of TMP+EC+DEC (v:v:v%, where v = volume) (see Table S1);
[b]: Coordination numbers of Li were calculated by multiplying the coordination ratios of the electrolyte solutions by their molar ratios;
[c]: Determined from the coordination number of lithium and the coordination ratios of the electrolyte compositions.

6. Supplementary discussion.

As reported in the main text of the article, Li-coordination by phosphates leads to an upfield shift of the ^{31}P signals due to a major degree of d-orbital occupancy in the P-O bonds once Li^+ ion is coordinated to O=P (Fig. S6). However, since such a d_π-p_π bond-back donation phenomenon does not take place in the carbonate species, the main contribution to the observed ^{13}C NMR outcomes derives primarily from electronegativity. Therefore, a deshielding effect has been observed from the free DEC/EC species to the Li^+-coordinated analogues (Fig. S4).

Corrections to the original diffusion NMR data presented in Supplementary Paragraph 4 have been carried out in order to minimize temperature and viscosity effects on the different solutions. In fact, it makes no sense to compare diffusion coefficients related to one (or more) species deriving from solutions that are different from each other in composition / concentration / ratio of their components. Solutions dissimilar for their composition or concentration may cause viscosity changes (and have different temperatures) affecting thus the corresponding diffusion coefficient values. A descriptive example is reported in Table S2 (third column) wherein the diffusion coefficient data for toluene differ considerably depending on the electrolyte solution in which toluene is dissolved, despite its mass is supposed to remain constant. Here, corrections to the original diffusion coefficient values allow several electrolyte solutions to be compared in a more accurate manner. Of note, toluene has now the same diffusion coefficient in all solutions (see diagram below Table S3). The diagrams gathered from Tables S3-S5 have been attained as follows. ^1H diffusion coefficients have been reported according to the Stokes-Einstein equation, 1, where D is diffusion coefficient, *k* is the Boltzmann constant, *T* is the temperature (in kelvin), η is the viscosity, and *r* is the hydrodynamic radius:

$$\mathrm{D} = \frac{k\,\mathrm{T}}{6\,\pi\,\eta\,r} \qquad (1)$$

By using toluene as internal reference, we can introduce a correction factor, Δ_X (2), corresponding to the ratio between the diffusion coefficient of toluene in the solution A and that in a solution X (with X = A to J, see the first column in Table S2). Since toluene slightly interacts with the polar electrolyte solution, the corresponding hydrodynamic radius (r_{Tol}) does not vary changing solution. Therefore, $r_{Tol\ A} = r_{Tol\ X}$ and the correction factors Δ_X appear as a constant that depends exclusively on the temperature and the viscosity of the two A and X solutions.

$$\Delta_X = \frac{\mathrm{D}_{Tol\,A}}{\mathrm{D}_{Tol\,X}} = \frac{\frac{k\,\mathrm{T}_A}{6\,\pi\,\eta_A\,r_{Tol\,A}}}{\frac{k\,\mathrm{T}_X}{6\,\pi\,\eta_A\,r_{Tol\,X}}} = \frac{\mathrm{T}_A\,\eta_X}{\mathrm{T}_X\,\eta_A} \qquad (2)^4$$

or $$\frac{\mathrm{T}_X}{\eta_X} = \frac{\mathrm{T}_A}{\Delta_X\,\eta_A} \qquad (3)$$

Diffusion coefficients for the electrolytes EC, DEC and TMP in the solution X ($D_{el\ X}$) can be determined according to a modified Stokes-Einstein equation (5):

$$\mathrm{D}_{el\,X} = \frac{K\,\mathrm{T}_X}{6\,\pi\,\eta_X\,r_{el\,X}} = \frac{K\,\mathrm{T}_A}{6\,\pi\,\Delta_X\,\eta_A\,r_{el\,X}} \qquad (4)$$

$$[\Delta_X\,\mathrm{D}_{el\,X}] = \frac{K\,\mathrm{T}_A}{6\,\pi\,\eta_A}\frac{1}{r_{el\,X}} \qquad (5)$$

If diffusion coefficients $D_{el\ X}$ (equation 4) rely on temperature, viscosity as well as hydrodynamic radius of the electrolyte in the solutions X, the modified diffusion coefficients (equation 5) are dependent exclusively on the hydrodynamic radius, since T_A/η_A is a constant. In this way, the effect of temperature and viscosity changes can be bypassed and a direct comparison of diffusion coefficients could be meaningful. We can display thus a diagram where "revised" ^{1}H diffusion coefficients (*i.e.* $[\Delta_X\ D_{el\ X}]$) have been related to the percentage of TMP (% vol.) in the solution X (see Table S3 and the below chart). Despite ^{7}Li and ^{31}P NMR spectra have not an internal standard (like toluene for ^{1}H NMR measures), a similar procedure however has been adopted using the same Δ_x correction factor already used for ^{1}H NMR DOSY experiments (see Tables S4 and S5).

Together with the chemical shift information, the self-diffusion coefficients obtained from ^{1}H, ^{7}Li and ^{31}P NMR DOSY enable us to more details on the Li^+ solvation. Concerning to the chart of ^{1}H Diff. *vs.* % vol. TMP, we can observe that ^{1}H TMP diffusion coefficients increase according to the percentage of phosphate in the electrolyte composition. This is due to the major portion of the free phosphate in solution, which is consistent with the α_{TMP} calculated in Table S6. A similar trend has been depicted in the chart ^{31}P Diff. *vs.* % vol. TMP, where ^{31}P Diff. of TMP molecules augments as the percentage of TMP increases. In the case of ^{7}Li Diff. *vs.* % vol. TMP, no meaningful changes of the ^{7}Li coefficient diffusions have been observed (the slight fluctuation of the data trend around 3.5 10^{-10} m^2/s may be easily related to the limit error of the DOSY technique). This indicates that the TMP concentration does not affect the diffusion and therefore the size of the aggregate around Li^+ is supposed to remain constant. Although we cannot provide a direct diffusion-molecular weight correlation from DOSY NMR data[5,6] (internal reference are not possible because of the shape and density of the electrolyte solutions), on the base of the literature,[7-12] we may postulate that the most plausible structure is a separate ion pair with a general composition $Li(DEC/EC)_x(TMP)_y$ (x+y=<4) according to the phosphate to lithium molar ratio (see Figure 2c).

Concerning the calculation of coordination ratio α and coordination number of Li (Tables S6 and S7 in Supplementary Paragraph 5), we followed a procedure already reported by Amine *et al*.[4]

Indeed, we suppose that the experimentally observed electrolyte diffusion coefficient in a Li-salted solution (D_{exp}) is the average of the diffusion coefficients of the electrolyte in dissociated ($D_{free\ el}$) and Li-coordinated form ($D_{Li\text{-}coord\ el}$), where α is the ratio of the coordinated electrolyte (equation 6).

$$D_{exp} = D_{Li-coord\ el} * \alpha + D_{free\ el} * (1 - \alpha) \quad (7)$$

Figure S10.

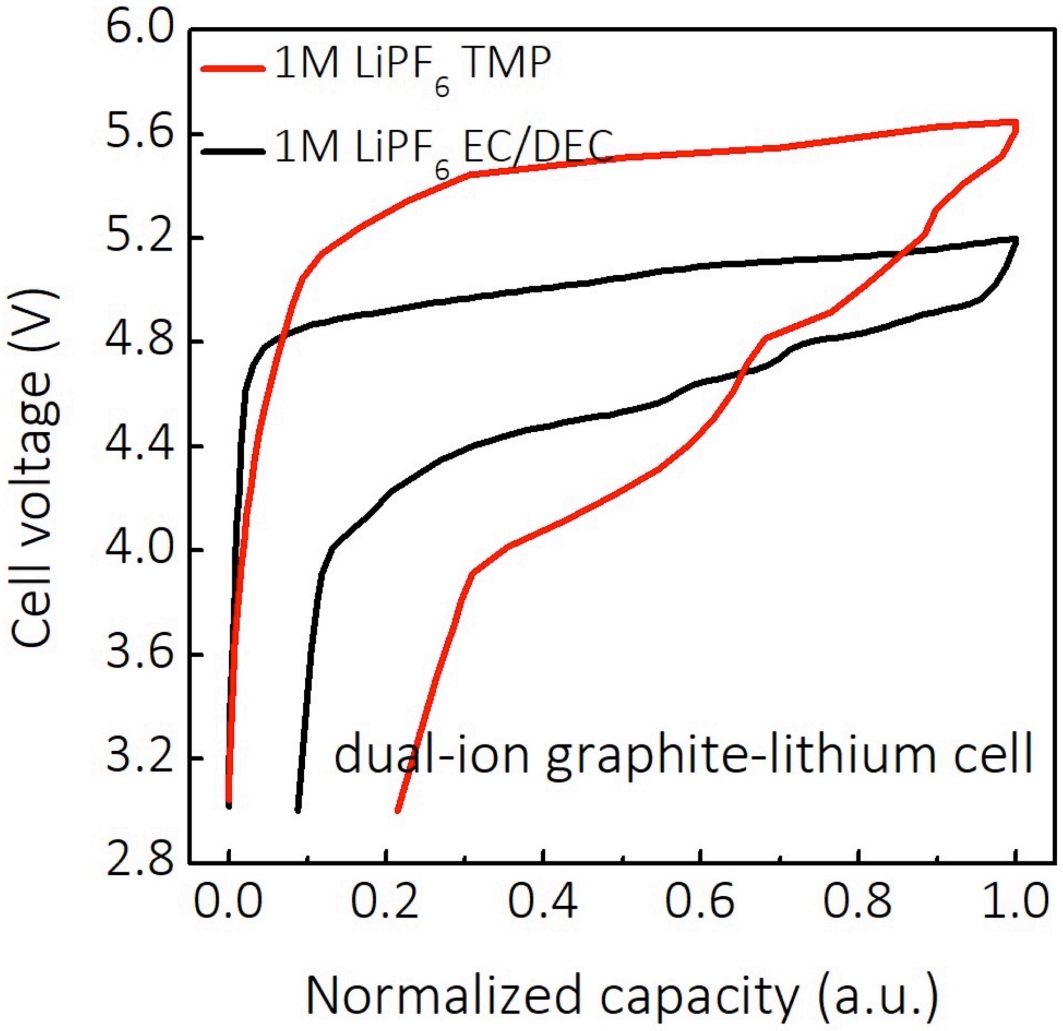

Dual-ion graphite-Li cells cycled with 1M LiPF6 in EC-DEC and TMP electrolytes. The higher polarization in the phosphate electrolyte is also the result of high solvation strength by phosphates resulting in poorer de-solvation kinetics of the lithium cations.

7. Supporting Information file Bibliography

(1) Vlad, A.; Rolland, J.; Hauffman, G.; Ernould, B.; Gohy, J.-F. Melt-Polymerization of TEMPO Methacrylates with Nano Carbons Enables Superior Battery Materials. *ChemSusChem* **2015**, *8*, 1692–1696.

(2) Chae, I. S.; Koyano, M.; Sukegawa, T.; Oyaizu, K.; Nishide, H. Redox Equilibrium of a Zwitterionic Radical Polymer in a Non-Aqueous Electrolyte as a Novel Li^+ Host Material in a Li-Ion Battery. *J. Mater. Chem. A* **2013**, *1*, 9608–9611.

(3) Kottam, P. K. R.; Kalkan, D.; Wohlfahrt-Mehrens, M.; Marinaro, M. Influence of Li-Salt Concentration on Redox Potential of Lithium Metal and Electrochemistry of Ferrocene in DMSO-Based Electrolytes. *J. Electrochem. Soc.* **2019**, *166*, A1574–A1579.

(4) Su, C.-C.; He, M.; Amine, R.; Chen, Z.; Amine, K. Internally Referenced DOSY-NMR: A Novel Analytical Method in Revealing the Solution Structure of Lithium-Ion Battery Electrolytes. *J. Phys. Chem. Lett.* **2018**, *9*, 3714–3719.

(5) Li, D.; Keresztes, I.; Hopson, R.; Williard, P. G. Characterization of Reactive Intermediates by Spectroscopy (DOSY). *Acc. Chem. Res.* **2009**, *42*, 270–280.

(6) Guang, J.; Liu, Q.; Hopson, R.; Kagan, G.; Li, W.; Monroe, T. B.; Williard, P. G. Conformational Polymorphism of Lithium Pinacolone Enolate. *J. Am. Chem. Soc.* **2016**, *138*, 15177–15188.

(7) Zeng, Z.; Murugesan, V.; Han, K. S.; Jiang, X.; Cao, Y.; Xiao, L.; Ai, X.; Yang, H.; Zhang, J.-G.; Sushko, M. L.; Liu, J. Non-Flammable Electrolytes with High Salt-to-Solvent Ratios for Li-Ion and Li-Metal Batteries. *Nat. Energy* **2018**, *3*, 674–681.

(8) Hwang, S.; Kim, D.-H.; Shin, J. H.; Jang, J. E.; Ahn, K. H.; Lee, C.; Lee, H. Ionic Conduction and Solution Structure in $LiPF_6$ and $LiBF_4$ Propylene Carbonate Electrolytes. *J. Phys. Chem. C* **2018**, *122*, 19438–19446.

(9) Ravikumar, B.; Mynam, M.; Rai, B. Effect of Salt Concentration on Properties of Lithium Ion Battery Electrolytes: A Molecular Dynamics Study. *J. Phys. Chem. C* **2018**, *122*, 8173–8181.

(10) Han, S.-D.; Yun, S.-H.; Borodin, O.; Seo, D. M.; Sommer, R. D.; Young, V. G.; Henderson, W. A. Solvate Structures and Computational/Spectroscopic Characterization of $LiPF_6$ Electrolytes. *J. Phys. Chem. C* **2015**, *119*, 8492–8500.

(11) Seo, D. M.; Reininger, S.; Kutcher, M.; Redmond, K.; Euler, W. B.; Lucht, B. L. Role of Mixed Solvation and Ion Pairing in the Solution Structure of Lithium Ion Battery Electrolytes. *J. Phys. Chem. C* **2015**, *119*, 14038–14046.

(12) Skarmoutsos, I.; Ponnuchamy, V.; Vetere, V.; Mossa, S. Li^+ Solvation in Pure, Binary, and Ternary Mixtures of Organic Carbonate Electrolytes. *J. Phys. Chem. C* **2015**, *119*, 4502–4515.